Computerized Ultrasonic Raytracing Model for C-scans of Solid Steel Bridge Pins

By

Sanjiv D. Parikh

Thesis submitted to the Faculty of the

Virginia Polytechnic Institute and State University

In partial fulfillment of the requirements for the degree of

MASTER OF SCIENCE

IN

ENGINEERING MECHANICS

APPROVED

_____

J. C. Duke, Jr., Chair

R. D. Kriz	**E. G. Henneke**	**W. E. Kohler**

August 6, 1998

Blacksburg, Virginia

Keywords: NDE, Ultrasonic Raytracing, Computerized C-scans

Computerized Ultrasonic Raytracing model for C-scans of solid steel bridge pins.

By

Sanjiv D. Parikh

Abstract:

This report describes the results of computerized ultrasonic C-scanning of solid steel bridge pins using a raytrace model. The raytrace model was developed to facilitate interpretation of data obtained from an ultrasonic C-scanning system for the Virginia Transportation Research Council (VTRC). The report discusses the reasons behind the development of the raytrace model, as well as specifications of the model, the input conditions, and the data output & visualization.

The model uses as input, various 'boundary' conditions of the solid steel pin with reduced diameter pin ends, as well as size and location information of a flaw or a wear groove placed within the main pin body. The model considers sound beams to be composed of rays and calculates ray reflections/conversions. This is done until the ray returns to a receiver location or is lost due to exceeding the time-of-flight. Once the model has returned with the received ray data, it uses the receiver conditions provided (transducer used, size of scanning grid, grid resolution, etc…), and calculates a 2-Dimensional C-scan image for each particular depth/time selected. Using PV-Wave visualization software, it is possible to plot the values for each depth to view a color graph. This graphical plot can then be analyzed/compared with the field C-scans to determine the closest match of a flaw or a wear groove inside the bridge pin. This helps in deciding if the condition of the pin is acceptable.

Acknowledgements

I wish to take this opportunity to express my heartfelt gratitude to Dr. John C. Duke, Jr., for his guidance throughout this study. I am indebted to him for his unwavering patience, encouragement and support. I have gained a lot from his knowledge and experience. I wish to acknowledge the support received from Virginia Transportation Research Council and Dr. Ron Kriz.

I wish to thank Dr. Ron Kriz, Dr. Edmund Henneke, and Dr. Werner Kohler for their assistance on my committee. I wish to thank Dr. Ron Kriz and the Virginia Tech CAVE for inserting the seeds of my future goals. I am very grateful to Mr. Robert A. Hunter for our close friendship for the past five years. I wish to thank my friend Mr. Aashish Jain for his help with suggestions on this report. I wish to thank my alma mater friend Mr. Jeffrey Thurman for encouraging the addition of "simple-ness" to my complex life. I also wish to thank Mr. Amit Goel, Mr. Baddy Hosur, and all of my unmentioned friends & colleagues for their support.

I would like to dedicate this document to my sister Chetal, half way around the world in India for her love and her faith in me to achieve my goals. I am unable to express to my father, and mother how grateful I am to receive their unconditional love and support throughout my existence. And for my elder brother, I just acknowledge him☺ (that is, for all the Intel inside info ;)).

Table of Contents

List of figures

List of tables

Chapter 1 Introduction

1.a History

1.a.1 National problem

The failure of a bridge is caused by the structure's inability to carry its design load. The failure might occur during the design life of the structure, causing injury or death to unsuspecting person(s). This problem is more prominent in older bridges, such as the ones having pin-linkage joints. This study deals with improving nondestructive evaluation of pin-linkage joints in bridges. Figure 1 shows an example of such a pin-linkage joint bridge structure.

There are 583,000 highway bridges (longer than 20 feet) in the United States. The safety of the motoring public depends on maintaining these bridges in good operating condition. With use, the condition of a bridge gradually deteriorates until repair, rehabilitation, or replacement is necessary. Reliable methods for assessing the condition of bridge structures allow bridge engineers to manage limited resources most efficiently. In situations where the condition of a bridge component is uncertain it is often necessary to assume “the worst-case” and replace the element. Steel bridge pins because of their nature are difficult to inspect due to lack of access to critical areas of the pin.

To overcome this lack of access an ultrasonic nondestructive evaluation method is used. The data obtained from this inspection procedure can be difficult to interpret due to the geometry of these pins, their contact with other bridge elements, and effects of wear. Efforts to improve the inspection data have been developed which involve scanning over the end of the pin rather than simply performing discrete hand-held measurements. The model developed here makes it possible to interpret the results of such scanning procedures.

Figure 1 Pin-Linkage jointed bridge span

1.a.2 Bridge pins in Virginia

In Virginia alone, there are hundreds of long-span bridges. Thirty-six of them are pin-linkage critically jointed structures. In a pin-linkage critically jointed structure, the bridge-span collapses if the pin or linkage assembly fails. Some of the pins and linkages in these bridges have had crack growth problems associated with them. Detection of linkage crack initiation and growth has been the subject of a previous VTRC report [Lozev, 97].

Table 1, lists all the pin linkage bridges in Virginia by district and structure numbers. Table 2 lists locations and their respective pin details available through Virginia Department of Transportation (VDOT.) There are other pin-linkage structures from table 1, for which no details were available.

Table 1 Pinned Bridge Structures in Virginia by Districts

Bridge structures in different districts can have identical structure numbers, listed below.

Salem	Bristol	Richmond	Suffolk	Stanton	Culpeper	No. Va.	Fredericksburg	Lynchburg
1010	1010	1048	2831	1015	1009	1042	1948	1939
1045	1032	1942	2816	1025		1112	1947	1901
1900	1042		2830	1015			1958	1987
1903			2833	1002			1959	1013
1082			6097	1191				
1037				1192				
1004				1019				
				1901				

Table 2 Virginia Steel Bridge Pin details in inch (cm) dimensions

District	Structure #	Material	Total Length	Main Diameter	Ends Length	Ends Diameter	Comments
Richmond	1942	?	11&1/8" (28.26)	6" (15.24)	1&3/4" (4.45)	4&1/2" (11.43)	Rte 147 over James River in Richmond/Henrico county
Richmond	1048	?	13&9/16" (34.45)	3" (7.62)	?	4&1/2" Butt	Rte 49 over Goodells creek in Mecklenburg county
Bristol	1032	AISI 4140	9&3/4" (24.76)	3" (7.62)	2&1/8" (5.40)	2" (5.08)	Rte 19 over Clinch River Tazwell county
Bristol	1042	A36	8&1/4" (20.96)	3" (7.62)	1&1/4" (3.18)	2&1/2" (6.35)	Rte 19 over Clinch River Tazwell county
Suffolk	2816	A588	8&5/16" (21.11)	4" (10.16)	1&5/8" (4.13)	3" (7.62)	Ramp C over Rte 64, City of Hampton
Suffolk	2830	A588	8&1/16" (20.48)	4" (10.16)	1&5/8" (4.13)	3" (7.62)	RampB over RampC NewMarket Crk & Rte 64, Hampton
Suffolk	2833	A588	7&9/16" (19.21)	4" (10.16)	1&3/8" (3.49)	3" (7.62)	Ramps A & B over NewMarket Creek Swamp, Hampton
Suffolk	6097	A7	16&1/4" (41.28)	3" (7.62)	1&1/8" (2.86)	2&1/2" (6.35)	Rte 684 over Nottoway River, SouthHampton county
Suffolk	6097	A7	6&5/8" (16.83)	3&1/2" (8.89)	1&1/4" (3.18)	2&1/2" (6.35)	Rte 684 over Nottoway River, SouthHampton county
Suffolk	6097	A7	7&1/4" (18.42)	3&1/2" (8.89)	1&1/4" (3.18)	2&1/2" (6.35)	Rte 684 over Nottoway River, SouthHampton county
Salem	1903	A257?	31" (78.74)	9" (22.86)	3&1/2" (8.89)	6" (15.24)	Radford Memorial Bridge, City of Radford
Salem	1903	A257?	29" (73.66)	10" (25.4)	3&1/2" (8.89)	6" (15.24)	Radford Memorial Bridge, City of Radford

1.a.3 Radford Memorial Bridge Pin

The Radford Memorial Bridge is a pin-linkage critically jointed non-redundant long span bridge. As with all bridges longer than 20 feet in the United States, it has been fully inspected biennially as per the Federal Highway Administration regulations (CFR23 650). Figure 2 shows the Radford Memorial Bridge. It was built in 1949, and has sustained substantial structural deterioration from environmental corrosion, which is obvious from a cursory visual inspection. As flaws started arising during routine ultrasonic inspection of its pins, the inspection frequency was increased. As of March 1997, 3 pins with detectable flaws were identified and repeatedly inspected every three weeks for assessing the flaw conditions.

Figure 2 Radford Memorial Bridge

Figure 3 shows a pin (called pin 12) in Radford Memorial Bridge. This pin has been the subject of particular concern, because of the configuration of the pin and the perceived location of the flaws based on the ultrasonic inspection. Therefore additional NDE had to be undertaken. The methods used to examine the pin, in addition to ultrasonic A-scan are listed here, and discussed later in this chapter: visual inspection, liquid penetrants, eddy current, x-ray radiography, and ultrasonic c-scans. The different methods produced conflicting results when compared for flaw descriptions in the pin.

Figure 3 Radford Memorial Bridge Pin #12

1.a.4 Literature review of pin ultrasonic testing and ultrasonic raytracing

Studies performed earlier indicate that angle beam testing could detect cracks closer to the outer diameter of the pin without allowing obstructions (such as cotter pin holes) to scatter the sound beam. [McCurdy, 1989] Guidelines for inspection, identification, and evaluation of fracture critical bridge members were established by Virginia Transportation Research Council to help plan, inspect, and document the testing. [Harland, 1986]]

Higher sensitivity transducers, compression waves, and other NDE methods have been used to aid inspection of Illinois bridge structures. [Harm, 1993] Instrumentation selection, methodology, results and testing confidence versus fracture mechanics prediction have been compared. The results and methodologies of various states have been reviewed and recommendations made. [Finch, 1994] A self-compensating ultrasonic system for flaw characterization in steel bridge structures was applied to inspection of pin connections. [Komsky, 1994]

The Pennsylvania Department of Transportation studied pin jointed structures and established testing criteria. Twenty structures were retrofitted to support failure of their pin-linkage assemblies, and three pin-linkage joint structures were made continuous. [Miller, 1994] Computerized imaging systems have been used for ultrasonic inspection of steel bridge structures. A-scan, B-scan, and C-scan techniques discussed, and evaluated experimentally. [Achenbach, 1996] Key elements of an effective inspection program, various transducers, influence of signal frequency, transducer diameter, and flaw identification have been discussed. [Gessel, 1996]

These studies have been a great help in transducer selection, field scanning system configuration, and basic understanding of ultrasonic inspection of steel bridge pins. However, none of these earlier studies were general enough to help in the setup of the C-scan raytrace model as developed in this study. EPRI (Electric Power Research Institute) has recently developed a raytracing software package called "Raytrace" which assists in the analysis of ultrasonic inspections of weld specimen. [EPRI, 1998]

1.b Motivation

1.b.1 Increase basic understanding of computerized ultrasonic reconstruction

Traditionally ultrasonic inspection of steel bridge pins has been limited to discrete A-scan measurements of time-of-flight and echo amplitude. The inspector was also able to estimate the transducer location used for obtaining the flaw related A-scan. For report purposes, and future comparison the actual A-scan is also often recorded. Definitions of A- and C-scans are given in Appendices A and B respectively. Recently Ultrasonic C-scanning systems have been developed for inspecting and monitoring flaws in steel in many different applications. Ultrasonic C-scanning can provide pin inspectors a significant advantage over ultrasonic A-scans when trying to identify flaws. Ultrasonic C-scanning provides an additional dimension to the reconstruction of flaw reflections (visual image representing a top down view of the flaw reflection planes.)

Flaw reflection planes are cross-sectional areas in the pin at depths where reflections occur. If the area of the flaw reflection plane is large, this indicates that the flaw could be large or that the flaw is oriented so that it can reflect from many different probe positions. In order to decipher the C-scan result of flaw reflection planes, some basic understanding of ultrasound propagation must be established. The raytrace model developed in this study applies an understanding of basic ultrasonic wave propagation for the situation involving a steel bridge pin with internal reflectors, including reductions in pin cross-section due to design or wear, or due to the presence of cracks.

1.b.2 Develop an integrated C-scan package to aid in pin inspection

Until now the pin inspector that performed ultrasonic NDE of pins did not have much of an objective tool to help his analysis of a flaw response, and had to depend on his ability to decode complex reflections from pin geometry and other interactions. The integrated C-scan package developed within this thesis can be used to help the pin inspector analyze and

understand test results. With this package the pin inspector can input a pin description with various geometric parameters including suspected flaws at different locations and can compare the results of the model to ultrasonic C-scans obtained in the field to help describe a flaw.

1.c Background on Radford Memorial Bridge pin.

1.c.1 Pin U8-LT-span-6 structural/environmental loading

The Memorial Bridge, designed in the 1940s, was not designed for the high volume of heavily loaded traffic that it presently supports. The pin-linkage joints in this bridge were designed so that the pin could rotate freely and allow one of the linkages to rotate from thermal expansion while the others remain attached rigidly to the piers. This bridge has two abutments, and six piers in-between. Two cantilever spans 428 feet each are fixed on three piers each. A single 117-foot long span hangs in-between the two cantilever spans supported by two pin-linkages for each span connection. There are also two pin-linkage-jointed spans at the outer ends of the cantilever spans that connect to the abutments. Each pin-linkage joint is composed of a top pin, a bottom pin, and a linkage member that is intended to rotate in-between the two pins. Figure 4 illustrates the Memorial Bridge pin-linkage joint of interest.

Figure 4 Radford Memorial Bridge Pin-Linkage joint

The top pin shown in Figure 4 above is currently under a large amount of stress, due to being frozen in place inside of the joint via corrosive elements leaching in between girder plates and the bearing surfaces of the pin. Severe corrosion has also resulted in the loss of structural material from the plates making up the joint, lowering the strength of the joint. Wear-grooves can form when girder plates transfer heavy loads over the small contact surface of the pin, wearing a small groove into its lateral surface. During ultrasonic examinations, these wear-grooves may be detected as flaws. An inability to separate flaws from wear-grooves causes confusion when analyzing C-scan images. Wear grooves do not propagate like cracks, and therefore are not as serious a threat to the structural integrity of the joint.

1.c.2 Ultrasonic inspection procedure

Virginia Department of Transportation (VDOT) uses the following procedure for ultrasonic inspection of steel bridge pins.

PROCEDURE FOR ULTRASONIC TESTING OF BRIDGE PINS

1 Scope

This test method outlines the procedure for ultrasonically determining discontinuities in bridge pins by the pulse echo method, using straight beam longitudinal waves induced by direct contact of the search unit with the material being tested.

2 Reference

2.1 ASTM E114-85 Ultrasonic Pulse Echo Straight Beam Testing by the Contact Method.

3 Personnel

3.1 Personnel shall be qualified in accordance with SNT-TC-1A Level II and certified by VDOT Materials Division.

4 Equipment

4.1 Instrumentation: Krautkramer-Branson Ultrasonic Pulse Echo unit, model USK-7 or equivalent.

4.2 Transducer: 0.50 inch (1.27cm) diameter, 2.25 MHz. (Angle-beam wedge, if applicable)

4.3 Couplant: Glycerin / cellulose gum with water added for desired consistency.

4.4 Reference Standard: Reference standard material and test pin material should be acoustically similar.

"NOTE: Equipment shall be qualified in accordance with AWS D1.5 Section 6, Part C.

5 Calibration

5.1 The ultrasonic unit shall be calibrated for distance on a standard of sufficient length and diameter to simulate the bridge pins being inspected. Sensitivity should be adjusted to a gain setting of at least 20 dB greater than that required for an 80% back-reflection from the end of the test pin.

5.2 Where the surface finish of the reference standard and the inspection item do not match, or where there is an acoustic difference between the standard and the inspection item, an attenuation correction shall be made.

5.3 Unless otherwise specified, the initial pulse and at least one back reflection shall appear on the screen of the CRT while testing for discontinuities in materials having parallel surfaces.

5.4 As a minimum, the calibration shall be checked each time there is a change of operators, when new batteries are installed, when search units are changed, when operating from one power source is changed to another power source, or when improper operation is suspected.

6 Testing Surface

6.1 Surfaces shall be uniform and free of loose scale and paint, discontinuities such as pits, gouges, dirt, or other foreign material which affect test results.

7 Scanning

7.1 Scanning may be either continuous or intermittent

7.2 Apply a layer of couplant, hold the search unit in hand and move slowly over the surface of the pin.

7.3 Scan pin from each end to insure full coverage whenever possible.

8 Test Data Records

8.1 District, Structure, County and Route.

8.2 Total pins, pin length and diameter.

8.3 Instrument description - make and model.

8.4 Search unit description - type, size, frequency, special shoe.

8.5 Pin location and indication information.

8.6 Pertinent instrument settings necessary to duplicate test.

8.7 Reference standards and degree of attenuation correction, if applicable

8.8 Operator

9 Evaluation

9.1 The procedure is limited in that the signals do not indicate the depth of the defect. it is also difficult to distinguish between sharp wear grooves and small initial cracks. Artificial reflectors, such as slots, may be added to the reference standard for signal comparisons when the results are inconclusive. Angle-beam testing may also be used to enhance the reflection of small outside diameter cracking.

9.2 The frequency of inspection will be as directed by the Structure and Bridge Division.

1.c.3 NDE inspection methods and their results for pin 12

Various inspection techniques were used in inspection of pin 12. These are detailed below with their results

Visual Inspection: This is the first step in the inspection of any bridge structure. In visual inspection, the inspector looks for visible cracks on the outer surface of the main pin body (further referred to as the pin's lateral surface). The amount of corrosion and material loss in the joint area is also observed. Rotation of the pin in the girder plates is compared from previous inspections (but the lack of rotation is looked upon more importantly).

In pin 12's case, visual inspection determined that the girder plates were experiencing severe corrosion/material loss and bleeding of these corrosives into the bearing area of the joint, freezing the pin in place. There was no rotation observed for this pin for more than the past three years. The lack of rotation on its own does not mean the joint is frozen and will fail. But this in

addition to corrosion observed at the plate contacts and bearing areas indicates a frozen joint. Inspectors usually leave paint marks lined up from the inner most girder plate to the outer lateral surface of the pin to use for observing rotation of the pin at the next pin inspection.

Liquid Penetrant: To do this test, the inspection crew had to remove the thick coat of paint coated on the lateral surface of the pin. A mini pneumatic jackhammer was used to accomplish this task. Once the old paint was stripped from the lateral surface, the liquid penetrant test was performed on the pin.

This gave the result of liquid penetrant testing on Pin 12, which showed no visual indication of cracks on the lateral surface of the pin.

Figure 5 Liquid penetrant testing results

Eddy Current: This method is very sensitive to surface cracks, and will often detect cracks too small to be observed by visual inspection or liquid penetrants.

In the case of pin 12, liquid penetrant testing was performed prior to eddy current testing. Jack-hammering applied in preparation for liquid penetrant testing had caused extensive dimpling on the pin's lateral surface causing any eddy current results to be inconclusive.

X-ray Radiography: This method is not widely used except in extreme cases. This is due to the high cost, as well as the handling of bulky apparatus needed to examine the pin. To further complicate the application of this method and in order to reduce the number of false indications/anomalies, it is necessary to close the bridge to traffic to prevent vibrations. One of the advantages of this method, though, is that it can show various views of a 3-dimensional object, giving a visual 3-dimensional representation of the flaw of interest. But a major disadvantage of this method is the anomalies resulting from any vibration of the source, the

object of interest, and/or the radiographic film. Therefore extraordinary preparations must be done before this test can be administered to minimize any vibrations.

As this test was performed on pin 12, an exposure of slightly over fifteen minutes was required. Three different views were taken. The radiographs had some indications but were blurred due to vibrations caused by wind and traffic travelling across the unblocked portion of the bridge. A clear flaw description could not be extracted out of the films.

Ultrasonic A-scan Examination: This method of examination is by far the most commonly used NDE method in finding flaw information in steel bridge pins. Ultrasonic examination uses sound waves travelling through a solid object reflecting when boundaries between regions with different acoustic impedance are encountered. The wave reflects from a flaw, shoulder, or pin end back to the top of the pin.

Sound propagates through a uniform homogeneous medium with uniform speed, so the distance a wave travels can be calculated linearly from the amount of time traveled. If the travelling distance associated with a returning echo corresponds to a location between the top and bottom shoulders of the pin then it is assumed to be associated with a flaw. Flaws are further investigated from the opposite pin face to confirm that the two travel distances correlate to a unique flaw location.

Ultrasonic A-scan examination on pin 12 from the upstream pin face detected three flaws while two flaws were detected from the down-stream pin face. Travelling distances of the flaws inspected from both pin faces do not correlate to reconstruct any flaws. There were two types of ultrasonic examinations performed on this pin. This report will discuss several possibilities of what type of flaw might be the outcome of the tests.

Ultrasonic C-scan Examination: The Ultrasonic C-scanning procedure and field scans of the bridge will be discussed in detail in the following chapter.

Chapter 2 Ultrasound C-Scanning (Flaw imaging)

2.a Ultrasound propagation in steel bridge pins

2.a.1 Introduction to ultrasonic waves

Many different ultrasonic testing methods have been developed for inspecting flaws in steel specimens including pulse-echo, pitch-catch, angle beam, surface waves, Lamb waves, etc. In this report the discussion will be restricted to pulse-echo, pitch-catch, and angle beam which are most appropriate for examining bridge pins. Ultrasonic waves have a frequency of 20 kHz or greater. Ultrasonic waves travel longitudinally (Wave propagates in a parallel direction to the direction of displacement oscillations) in steel at a speed of 5190 m/s (204,000 in/s.). Ultrasonic waves travel transversely (i.e. Wave propagates perpendicular to the direction of the displacement oscillations) in steel at a speed of 3230 m/s (127,000 in/s.) [Bray, 97]

2.a.2 Snell's Law

When an ultrasonic wave, as characterized by a ray, encounters a boundary between two media with different acoustic impedances, the disturbance that results is one that is physically consistent with the nature of wave propagation in the material as well as being consistent with the conditions of the boundary. Mathematically this would suggest the resulting disturbance must satisfy the equation of motion, and satisfy the boundary conditions. Generally the boundary between a solid and air, is considered a “free” boundary. In order to satisfy the above conditions, incident longitudinal and vertically polarized shear waves need to reflect from the boundary. The departure of this addition, and opposite mode is referred to as mode conversion. For isotropic materials it can be shown that a relationship, analogous to that of Snell’s Law for optics, describes the relationship between wave speed and angle of incidence, and reflection. Equation 1 shows that the angle (with respect to the normal to surface of impact) of the reflected wave is dependent on the angle of the incoming wave (w.r.t. normal), where the subscript i is for incident waves, Lr is for longitudinal waves, and Lt is for transverse waves.

$$v_i / \sin\theta_i = v_{Lr} / \sin\theta_{Lr} = v_{Lt} / \sin\theta_{Lt}$$

Equation 1 Snell's Law

2.a.3 Interaction of the ultrasonic wave and a boundary

If the boundary value problem for an elastic ultrasonic wave incident on a free boundary of an isotropic material is solved it is possible to describe the relationship between the amplitudes of the reflected longitudinal and shear waves as a function of the amplitude of the incident wave. The results depend on whether the incident wave is longitudinal, or shear, and the angle of incidence. [Kolsky, 63] It should be noted that shear waves polarized horizontally relative to a boundary experience no mode conversion when interacting with a free boundary in an isotropic material.

2.b Calibration pin

2.b.1 Details of calibration pin fabrication

Appendix A and B present a detailed explanation of A-scans and C-scans respectively. To develop the capability for performing an ultrasonic C-scan examination of the Radford Memorial Bridge pins, a calibration pin was fabricated. The calibration pin was formed out of a solid steel cylinder 9" in (22.86cm) diameter with two ends machined off at 6" in (15.24cm) diameter. The ends were 3.5" in (8.89cm) depth. Prior to imbedding any flaws in this pin, ultrasonic A-scan and C-scan examinations were performed as shown in figure 6a, to detect any manufacturing defects already present within the stock material. Figure 6b shows that no extant flaws were detected from ultrasonic testing.

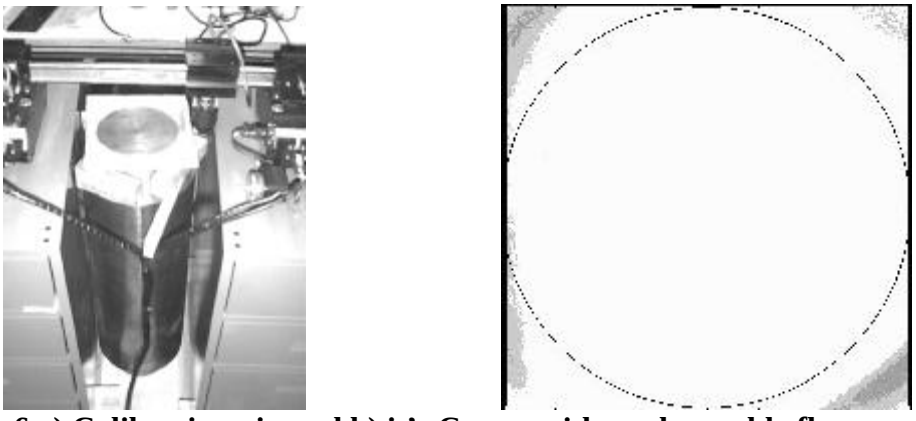

Figure 6 a) Calibration pin and b) it's C-scan with no detectable flaws present

The calibration pin had been imbedded with two flaws. Flaw one being a surface breaking flaw, and flaw two, a sub-surface/slag flaw.

To imbed the sub-surface flaw, the pin material (steel) was excavated from the area directly above the flaw position on the pin's lateral surface. A steel rod was welded into the cavity left by the excavated material. The rod was notched close to the welded area. When fatigued, the notch grew into a crack, and cracked completely through the rod. The cracked region of the rod was then cut and placed back onto its mating crack inside of the cavity. The mated crack pieces were then reattached by welding around the crack, so as to preserve the physical crack (air gap within steel.) Once the crack was sealed, the excavated region was filled with weld metal and the pin surface restored by machining, shown in figure 7. The Surface-breaking flaw was imbedded in much the same way. The calibration pin inclusions were ultrasonically verified to match the details shown in figure 8.

Figure 7 Calibration pin after flaw insertion

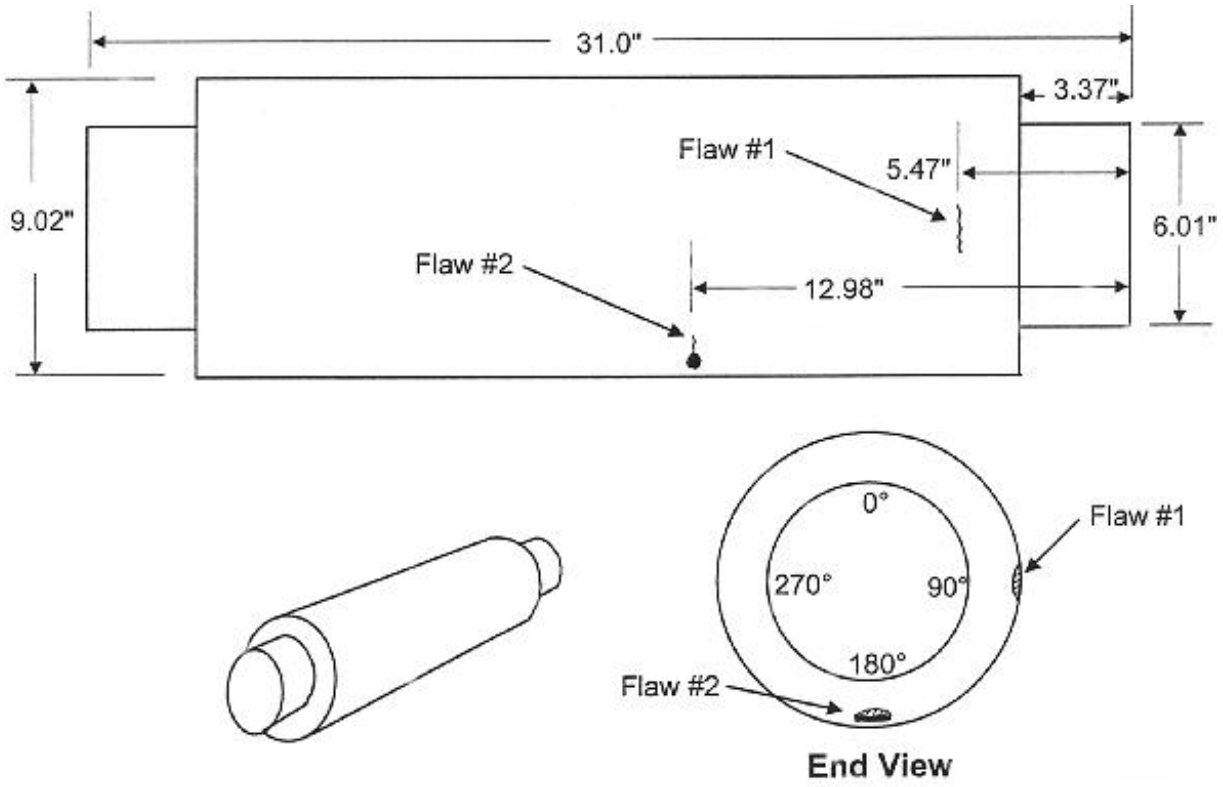

Figure 8 Flaw details in calibration pin

2.b.2 Samples of A-scans of calibration pin

Figure 9 shows an A-scan of the calibration pin after insertion of the two flaws. The test shows the slag flaw as a peak in-between the reflections from the top and bottom shoulders. The flaw depth is indicated in the image as 13.276 inches (33.72cm) below the top pin face.

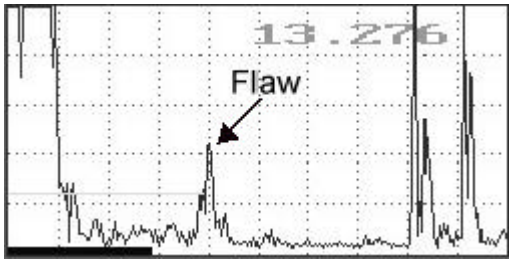

Figure 9 A-scan of calibration pin detecting flaw

2.b 3 C-Scan of calibration and bridge pin

Figure 10 shows a C-scan of the calibration pin at the depth indicated in the above A-scan (13.276 inches (33.72cm)). The flaw is shown as the dark area.

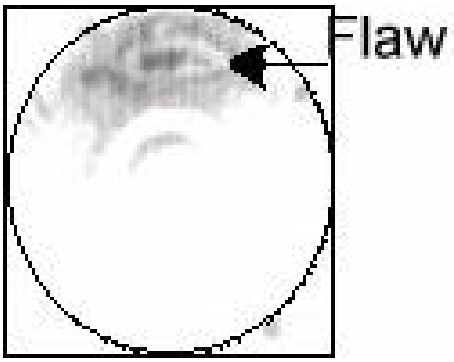

Figure 10 C-scan of calibration pin indicating flaw

C-scanning a pin face utilizes an ultrasonic C-scanner. The transducer moves horizontally until the edge of scanning area is reached. The magnetic roller drive then moves the whole scanner vertically down an increment, and the horizontal scanning begins again. This process repeats until all of the scanning area is examined.

In order to C-scan pin 12 on the Memorial Bridge a special automated scanning system has been used, shown mounted to the pin-linkage joint in figure 11. The system consists of the following components:

- A robot scanner unit;
- A 2.25MHz, .546" (1.387cm) diameter Kraut-Kramer ultrasonic transducer;
- An Infometric Pentium class computer with a Sonix 8100 DAC, a pulser-receiver board, all mounted inside a compact field specific case;
- The controller unit of the robot;
- Mounting assembly with iron tracks bolted on to accommodate the magnetic roller drive system of the robot.

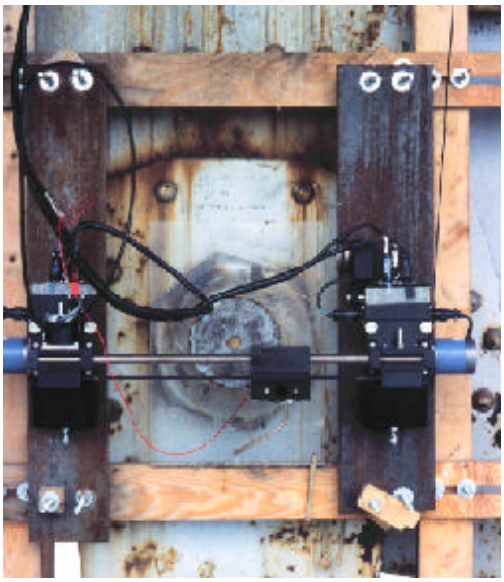

Figure 11 Shows the robot pin scanner attached to the joint.

The robotic system used on the Memorial Bridge is complex and needed to be setup and calibrated prior to scanning. Due to the scanning surface (pin face) being vertical, it was particularly difficult to keep the couplant in between the probe and pin. Without appropriate coupling, the maximum amount of ultrasonic energy will not be transferred between probe and pin, ultimately reducing the signal strength of any echoes. The bridge inspector had to manually spread the couplant at periodic intervals to continuously maintain a layer of couplant on the pin face. The C-scanning software of this system is limited in that, signals are not saved for later processing, rather the signal in the time gate is averaged and its amplitude is discretized, and used to form an image as the final output.

Chapter 3 Modeling

3.a Introduction to the model

3.a.1 Introduction

Complications arise because pin shoulders limit access. Hence, beam spread is relied on during ultrasonic pin inspection to detect flaws. This broad beam causes reflection patterns from the pin geometry that are not easy to interpret correctly. This raytrace model was designed to simulate complex/multiple reflections and show the resulting C-scans of suspected flaws.

As with any computer-based model, limitations are imposed by the computing system capabilities. As such, some of the limitations of the model include: Inability to model non-planar flaws, inability to handle more than one flaw simulated at any time, computationally limited (memory limitations, slow file accessing and periodic memory overflow problems.)

3.a.2 Advantages of the raytrace models:

These models can be used to calculate different configurations of flaw sizes and locations. The models allow the size and shape of the flaw and its location to be entered as input parameters giving the ability to locate the flaw and or change it's size.

Scanning can be done using a variety of different probe configurations. Probe data (probe size, beam spread angles, and probe locations) are also variable parameters entered into the models, allowing the inspector to try different probe configurations which may give more insight into complicated reflection patterns.

3.a.3 The disadvantages of models:

This model only considers longitudinal and transverse bulk waves. Surface waves and other modes are ignored because the pin inspectors cannot physically observe their interactions in the bridge pins.

The flaw is only a planar flaw in the Z-dimension (axial dimension), i.e., the flaw has constant z-position. Models were designed around a Z-plane flaw because cracking in steel pins due to shearing are the inspector's (researcher's) main detection concern. Flaws produced by shearing forces have been taken to be planar cracks slicing at the cross-section of the pin. Modeling an inclined plane crack within a cylindrical pin is a possible extension of this study.

The threads from the main bolts that fit the pin onto the joint plates are not modeled due to the continuous non-planar thread angle with complicated geometric description. Also, the cotter pin hole inside the shoulders has not been modeled due to its complexity, a continuous circular cylinder inserted perpendicular to the axis of the main pin cylinder.

3.b Philosophical basis for a raytrace model: Beam modeled as a point source

The ultrasonic beam is assumed to be composed of tiny rays, which emanate from a collection of point sources. Although the number of rays composing a beam can theoretically be infinite, a large, but finite number were expected to be sufficient for engineering analysis. In this model the beam diameter has been assumed to be the diameter of the transmitting probe. Each ray consists of an origination point, amplitude, a phase angle, and the direction of propagation. The behavior of rays within the pin is governed by ultrasonic wave propagation.

3.c How the model handles reflection, mode conversion, and new ray generation

3.c.1 Characteristic wave speed

Since time-of-flight and length-of-travel are synonymous in this model, when a ray mode converts from longitudinal to transverse, it's time-of-flight increases due to change of wave speeds. Because this model uses a linear relationship between time-of-flight and length-of-travel, the amount of length traveled as a transverse ray is multiplied by a characteristic speed factor. That factor is the ratio of speed of longitudinal wave over speed of transverse wave in steel. When a ray changes mode from longitudinal to transverse, it takes longer time to reach the same distance as if it were longitudinal. So the length that is traveled as a transverse ray is the length that it would have traveled as a longitudinal ray multiplied by the characteristic speed factor. This factor is less then one for rays converting from longitudinal to transverse and is the inverse for rays converting from transverse to longitudinal.

3.c.2 Reflection

Reflection occurs when a ray interacts with a boundary. Knowing angle of incidence and the speed of wave propagation in a medium, reflection angles can be determined from equation 1, Snell's law.

3.c.3 Mode conversion

Mode conversion normally occurs when an incident ray hits the surface at an angle less than 90 degrees, and reflects a ray of the opposite mode. The only mode conversion that is considered valid for this model is that occurring at the corners, where an incident ray hits the lateral surface, mode converts, and immediately hits a flaw, groove, shoulder, or bottom and mode converts back to original mode.

3.c.4 Ray generation cases

When a ray hits the reflector at an angle not equal to 90 degrees, some energy goes into a reflected ray of the same mode, while other part is used in generating an additional "child" ray of the opposite mode, this is called new ray generation. If one formulates the boundary value problem for a stress wave incident on a stress free boundary [Kolsky, 63] and then solves for the reflected and mode converted amplitudes, equations 2, 3 result for incident longitudinal and equations 4, 5 result for incident shear waves. Figure 12 illustrates this boundary value problem and it's variables.

$$A_2 = A_1[\frac{2Cos(a_1)Sin^2(b_2)Tan(2b_2) - Cos(2b_2)Sin(a_1)}{2Cos(a_1)Sin^2(b_2)Tan(2b_2) + Cos(2b_2)Sin(a_1)}]$$

Equation 2 Amplitude of reflected longitudinal wave

$$A_3 = 2(A_1 - A_2)[\frac{Cos(a_1)Sin(b_2)}{Cos(2b_2)}]$$

Equation 3 Amplitude of mode converted shear wave

$$B_2 = B_1[\frac{Cos^2(2b_1)Tan(a_2) - 2Sin(2b_1)Sin^2(b_1)}{Cos^2(2b_1)Tan(a_2) + 2Sin(2b_1)Sin^2(b_1)}]$$

Equation 4 Amplitude of reflected shear wave

$$B_3 = [\frac{(B_1 - B_2)Cos(2b_1)}{2Sin(b_1)Cos(a_2)}]$$

Equation 5 Amplitude of mode converted longitudinal wave

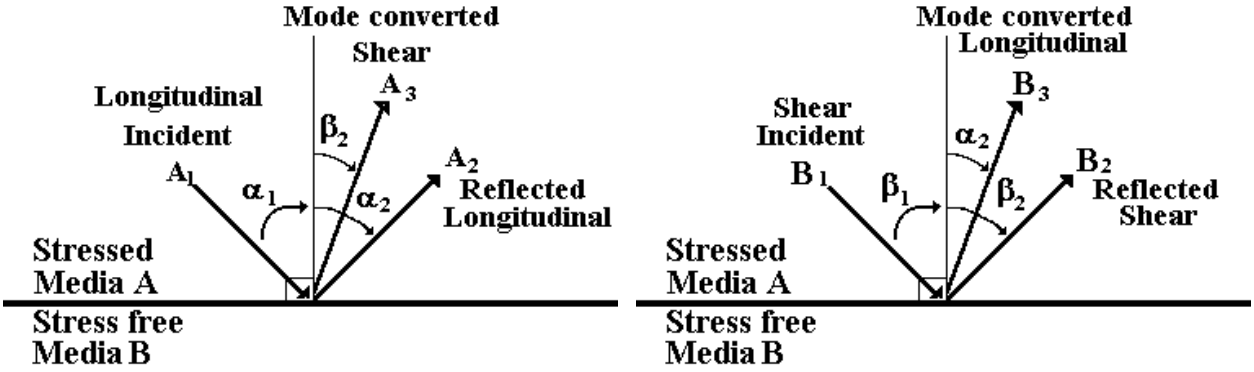

Figure 12 a) Illustration of incident longitudinal and b) shear wave intercepting a stress-free boundary.

Chapter 4 FORTRAN program

4.a Programs (chronological description of the interface algorithms)

4.a.1 Core kernel

All three interface modules, A-scan, C-scan, and forward scatter algorithms are overlays that interface with the kernel as shown in figure 13a. The kernel is the core process of the program. Given a ray direction vector and origin point, the kernel calculates the reflections, interactions, and truncations. It also returns the data back to the interface algorithms for further filtration and processing as shown in figure 13b.

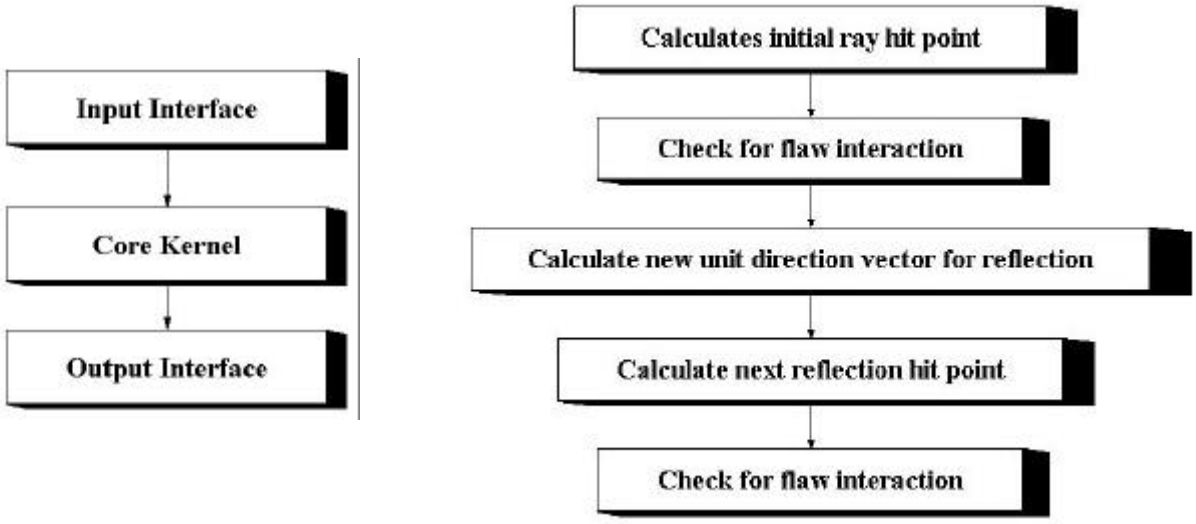

Figure 13 a) Flow chart of main program. b) Flow chart diagram of core kernel processes

4.a.2 Description of the A-scan interface algorithm

The FORTRAN program which implements the A-scan algorithm was developed to give the inspector a quick plot of reflections returning to the probe on the pin face. Flow-charts Ascan.cht, hitcalc.cht, dirvect.cht, crackint.cht, truncate.cht in appendix D contain detailed data flow paths for the A-scan algorithm. Appendix F describes the list of input parameters that must be entered into the program for it to execute properly. The output file Ascan.dat will be discussed later in the detection-visualization chapter. This executable program will generate rays from a single probe fixed at a particular location. The down angle refers to the angle between the ray and the pin-face surface which is perpendicular to the cylindrical axis. The circular angle

refers to the (clock) angle that can be observed by an axial view of the pin, positive when sweeping counterclockwise from 0 to 360 degrees. Figure 14 illustrates down and circular angles. The rays are generated starting with the widest down angle incrementing until the ray is pointing 90 degrees (straight down), incrementing from 0 to 359.99 degrees in circular increments for each down angle increment. All reflections returning to the top of the pin face are checked for distance from probe, if within probe radius, then the top-hit-point data is written to the output file ascan.dat.

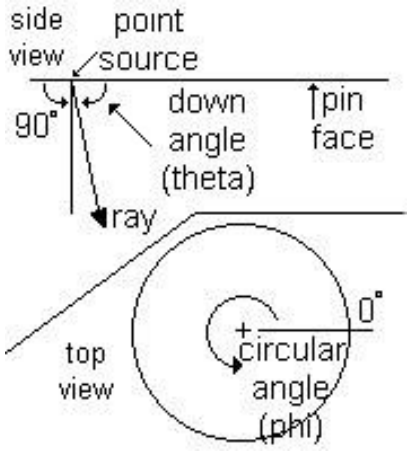

Figure 14 Definition of relevant angles used within the algorithms

The following list of parameters can be varied to better understand how the model is affected by these parameters. For example, increasing the crack dimensions from 6.4 degrees to 64 degrees affects the number of rays that will reflect from the crack. Changing beam spread angles, crack size, location, and probe location affects the outcome of the results.

PROBX: probe x coordinate location

PROBY: probe y coordinate location

SPRBEG: begin downward-ray-angle (68 degrees)

SPREND: end downward-ray-angle (89.9 degrees)

DWNINC: downward-ray-increment-angle (.5 degrees)

PHIBEG: begin circular-ray-angle (0.0 degrees)

PHIEND: end circular-ray-angle (359.99 degrees)

CIRINC: circular-ray-increment-angle (.2 degrees)

CRANGS: begin crack-angle (-3.2 degrees for subsurface flaw)

CRANGL: end crack-angle (3.2 degrees)

CRRADS: crack small radius (4.19 inches (10.64cm))

CRRADL: crack large radius (4.44 inches (11.28cm))

CRHIGH: crack length in z plane (13 inches (33.02cm))

PDIAM: probe diameter for A-scan (.545 inches (1.38cm))

4.a.3 Description of the back-scattered C-Scan interface algorithm

The flow-charts Cscan.cht, hitcalc.cht, dirvect.cht, crackint.cht, truncate.cht in appendix D contain detailed data flow paths for the C-scan algorithm. This model will allow the use of probes having beam spread ranging from focused beam (spread angle of almost 90 degrees down angle) to probes with wide beam spread (60 degrees down angle). The flaw can be adjusted to various sizes and locations placed within the main cylinder of the pin. These adjustments can be made by changing the crack parameters (CR****) listed below. The probe ray-generating grid can also be changed to fit available computational resources. For example, a smaller grid (13-24 nodes squared) to a medium-high resolution grid (98-192 nodes squared) can be entered into the program through the N by P parameters. As with the A-scan program, the probe diameter (PRDIAM) can be changed to test different size transducers.

To generate results similar to the calibration pin C-scans, the correct parameters must be entered into the code by the input2.dat file. The following is a brief description of the important input parameters.

SPRBEG: begin downward-ray-angle

SPREND: end downward-ray-angle

DWNINC: downward-ray-increment-angle

PHIBEG: begin circular-ray-angle

PHIEND: end circular-ray-angle

CIRINC: circular-ray-increment-angle

CRANGS: begin crack-angle

CRANGL: end crack-angle

CRRADS: crack small radius

CRRADL: crack large radius

CRHIGH: crack length in z plane

N: x row incrementation number [x-grid value]

P: y column incrementation number [y-grid value]

PDIAM: probe diameter for C-scan

4.a.4 Description of the forward scattered image (groove) interface algorithm

The forward scattering algorithm is designed to be a quick indicator of a flaw interacting with rays. It uses the A-scan algorithm's kernel to calculate rays interactions, but like the C-scan algorithm, it adds a new dimension to detection. This program generates rays from multiple points within the probe instead of a single point source like the A-scan and C-scan algorithms. It accomplishes this by establishing a "virtual-point" at the center of the probe on top of the pin face. A virtual-point, shown in figure 15, is a point that extends in the Z-direction, forming point sources above the pin face instead of on the surface of the pin face, generating rays at a fixed down-angle, creating symmetric cones emanating down from a particular length. For example, ten virtual-points over the probe point would generate ten cones stacked one on top of the other, all generating rays at a fixed down-angle. As these cones intersect the top surface of the pin face they form rings about the probe center point. Flow-charts fwdscatr.cht, hitcalc2.cht, dirvect.cht, grvintcp.cht, truncate.cht in appendix D contain the detailed data flow paths for the forward scatter algorithm.

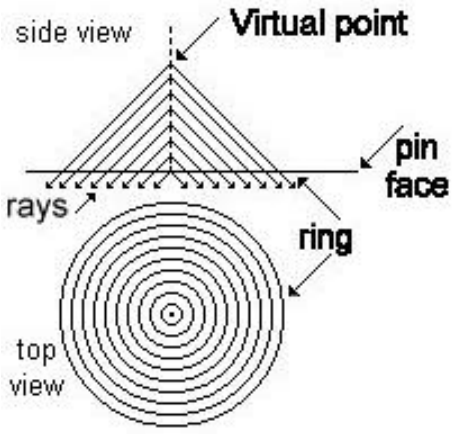

Figure 15 Shows virtual-point and the rings formed by virtual cones

The forward scattering program uses the same parameters as the A-scan and the C-scan except with these few additions. The groove parameters (GR****) describe the groove (keyed

slot running perpendicular to the pin axis around the main pin cylinder) size and location on the pin. The beam spread, however, is restricted to a fixed down angle, similar to a read safety pylon, that angle is chosen by entering in a value for parameter THETA. This model generates its rays from a single probe point with multiple radii (rings) and all rays' Z-unit vector remaining unchanged (fixed down angle). The parameter that governs how many rings are inserted within the probe diameter is RINGOT. The greater the number of rings the greater, the higher the cone density, resulting in higher ray density per probe. The forward-scattered rays are detected at the bottom of the pin. The rays, however, do not have to be within a probe diameter's distance away from the projection of the generating probe on the top of the pin. Rays can be collected at any X-Y position on the bottom of the pin.

PROBX: probe (virtual point) x coordinate location

PROBY: probe (virtual point) y coordinate location

GRVTOP: the z position of top of groove (13 inches (33.02cm))

GRVBOT: the z position of bottom of groove (13.5 inches (34.29))

GRVDPT: the radial depth of the groove (.5 inches (1.27cm))

THETA: the central-down-angle for the probe (75 degrees)

RINGOT: the number of rings that makeup a transducer (15 rings)

4.b Geometrical description of the cylindrical pin

4.b.1 Development steps

To model the solid steel bridge pin properly in the FORTRAN program, development of the program was broken down into several major sections: basic cylinder, addition of shoulders, addition of crack flaw, and addition of grove slot.

4.b.2 Basic solid cylinder

Initially, a solid steel circular cylinder of large length to radius ratio was modeled. Shown in figure 16, the basic circular cylinder consisted of a pin of length of 31 inches (78.74cm), and diameter of 9 inches (22.86cm). This cylinder was embedded into the routine as two planar surface areas and a lateral surface area.

Figure 16 Basic cylinder of length L

4.b.3 Addition of shoulders

Once this routine modeled the raytrace behavior properly and reflected the rays according to the governing reflection equations, shoulders at each end were inserted and the model was filtered for computational errors. The shoulders were added as smaller sections of the main cylinder with each at a length of 3½ inches (8.89cm), and diameter of 6 inches (15.24cm). As shown in figure 17, the shoulders were modeled as a circular plane of 9 inches (22.86cm) diameter with a 6 inches (15.24cm) diameter circular area cut out from the center. The reflections were calculated using the same governing equations as the top and bottom pin surfaces. The length of the main cylinder was reduced to 24 inches (60.96cm).

Figure 17 Basic cylinder with pin ends

4.b.4 Addition of flaw

The model correctly reflected the rays for a steel pin without any flaws, wear grooves, or any other obstructions. To aid in flaw identification, a flaw was then added. The flaw can only be a planar flaw in the Z (length) dimension to work properly in the routine. The current flaw is a pie cut of a circular arc, as illustrated in figure18. Dimensions of the current flaw are simulating the dimensions of calibration pin's sub surface flaw with slag. The flaw can be placed at any length in the main diameter and at any circular angle from zero degrees respective to the X-Y axis.

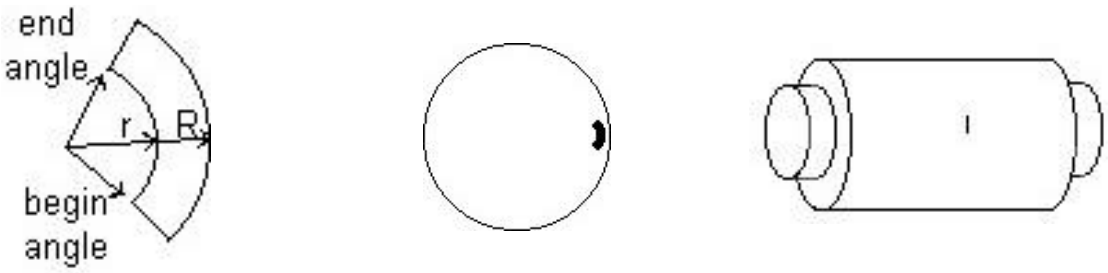

Figure 18 Defined slag inclusion crack in basic pin

4.b.5 Addition of the wear groove

The wear groove was added into the routine, to test if any differences can be observed in the ultrasonic results between the groove and the flaw, which might be used to develop a NDE procedure that allows inspectors to reliably differentiate between wear grooves and shear cracks. The groove description is the same as the flaw, except that, instead of a planar pie slice in the circular area, it is similar to a shoulder that is keyed into the main cylinder's diameter, shown in figure 19. The groove can be placed at any length location, be of any thickness, and of any diameter depth.

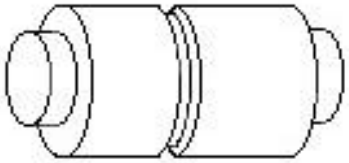

Figure 19 Basic pin with wear-groove (keyed slot)

4.c Post-processing (output)

4.c.1 Definition and format of main output of C-scan program.

The data output from the main program is listed in detail by columns within the output.dat file. For each X-Y probe ray-generating position on the grid, columns of X and Y position of the ray arrival at the top surface, the ray's total length (divided by two), it's circular angle, and it's total reflections are listed in a row for each arrival. The amount of data being written to file depends on the grid resolution chosen in the input file. The grid contains X number of rows by Y number of columns. Nodes of the grid represent the allowed probe positions during the scan. For example, if there are 10 rows by 10 columns, there are 100 possible probe positions in this rectangular scanning area, but the probe will only generate rays

for the positions that are physically on the pin face. To encompass the circular pin face area, the C-scan model assumes a square-scanning grid, with sides greater than the pin face diameter.

The data collected represents reflections that return to top of the pin face within the probe area. These points are used in calculating the amplitude of the A-scan signal at their respective discretized depths. If 256 depth intervals are chosen for a 31-inch (78.74cm) long pin, then a C-scan at any particular depth will have a thickness of .121 inches (.307cm). An inch (2.54cm) of thickness for C-scans is considered medium in resolution for this model due to the amount of computation required for higher resolutions.

For example a medium resolution grid, 192x192 probe points total to 36864 possible probe locations. From each probe point the code checks to see if that point is physically on the circular pin face. Once a point on the face is reached, for each down angle iteration (58 degrees to 89.99 degrees), a circular incrementation from 0 degrees to 360 degrees is performed. For each of those circular iterations, the code calculates 6-10 reflections. The total number of reflections range near four and quarter trillion reflections for a medium-resolution grid C-scan output file. Condensed data storage (which only stores valid rays that reached the pin face within probe diameter from generating point) for this resolution ranges near 128 megabytes. Processing output files of such resolutions consume massive computer resources as well.

To reduce the computer time spent reading rows of data of output.dat file, a performance-optimized post-processing algorithm is used. For each ray collected, the algorithm compares the separation distance between a point of ray generation and the receiving-probe-center, which must be less than or equal to the probe diameter. Once they are valid source and receiver sites, as shown in figure 20a, the received ray is compared to the receiving probe center point to check if their separation distance is less than or equal to probe diameter. If both the checks are passed, as shown in figure 20c, the ray's amplitude of one is assigned to the receiver node point at the ray's discrete length section. Using this method of ray collection, one single generated ray can be detected by many receiving probes.

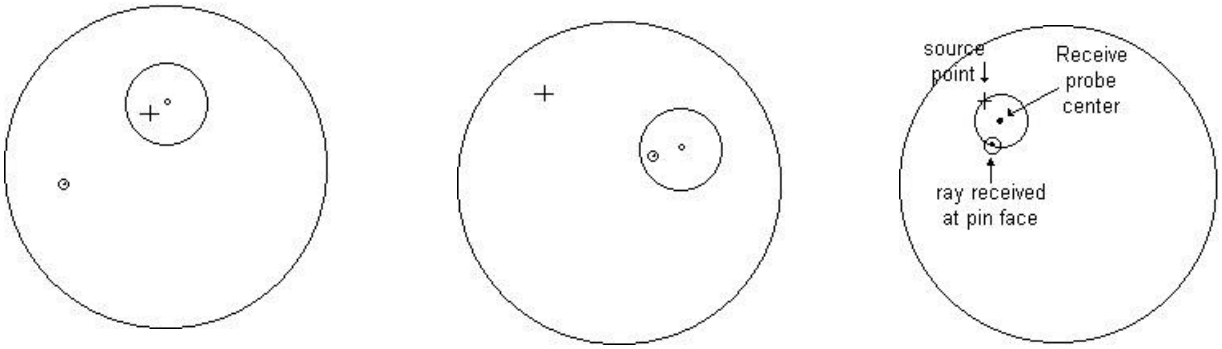

Figure 20 a) Illustrates a valid source and receiver probe point, b) a valid detected ray and receiver probe point, and c) a valid source, receiver, and detected ray

4.c.2 Processing of main output for specific receiver

The main output once calculated can be post processed for many combinations of receiver grid configurations, from a very course grid to a very high-resolution grid. The effect of which can be seen in the following figure 21 (a,b), two different resolution receiving grid plots of the same generated rays. The high-resolution grid receiver scan shows more flaw reflection detail when compared to its low-resolution counterpart.

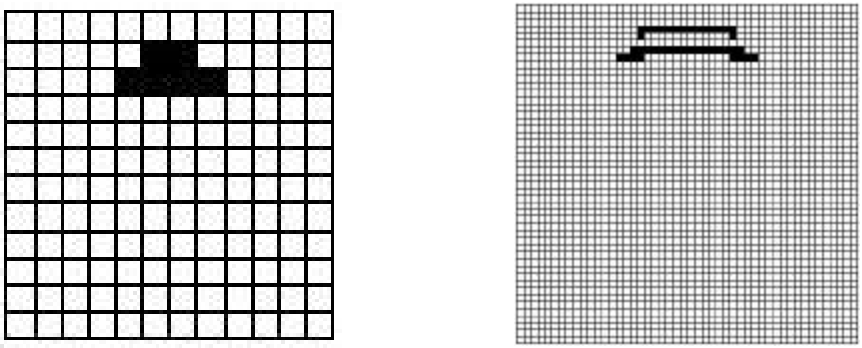

Figure 21 a) Low-resolution, and b) medium-resolution receiving grids

Chapter 5 Detection and Visualization

5.a Detection by A-scan

Detection of a flaw, using the A-scan FORTRAN program was accomplished by locating the receiving probe in the same position on the pin face as the ray-generating probe. This type of transmission/collection technique is called pulse-echo. For an A-scan, rays returning to the top of the pin face must return inside the probe's diameter to be counted valid. The pin length is discretized into n sections, each of equal length. All valid rays are assigned an "amplitude" value of one. Each valid ray is assigned into a discretized length section, adding one to its previous amplitude total. The amplitude totals are plotted against their respective length sections to result in a modeled A-scan image.

5.b Detection by C-scan

Flaw detection using the C-scan algorithm is accomplished by post processing the generated data through a receiving grid. During ray generation, a MxM grid is used, where each of the nodes act as point sources. The receiving grid contains NxN nodes, a subset of those NxN nodes represents the receiving transducer. To reduce time spent rereading the millions of rays collected within a single C-scan main output file, the reflected rays must return within a probe diameter from the point of ray generation. This allows a small number of nodes to generate rays that can be received by a larger number of nodes, allowing a higher resolution C-scan image to result. For example, a C-scan using 24 by 24 ray-generation nodes is collected using a 96 by 96 node grid scanning over a 6 inch (15.24cm) by 6-inch (15.24cm) area.

In order to generate a C-scan from the data output by the FORTRAN programs, the data must be filtered for proper ray returns. The collection and filtration of the returning point data is accomplished through the post-processing FORTRAN program called "post3.for" which implements a transducer receiver algorithm. The post3 algorithm reads in point X-Y position and its length from output.dat file, and iterates through all receiving nodes to check how many probe locations will pick up this ray within a probe diameter of the probe point generated it. This iteration occurs for each and every probe point within "output.dat" data file, so fewer rays can be generated and at the same time can count for multiple receive points due to the fact that

more than one probe position falls within a probe diameter when receiving with high-resolution grids. This means one probe location generates the rays but four probes can receive part of those rays as they are scanning. This reduces the number of generating nodes needed to scan a region by the model.

5.c Detection by Forward scattering

The forward scattering program uses the pitch-catch technique, in which a probe at the top pin face generates the rays while a probe on the bottom pin face, receives the reflections. To compare C-scans (backscatter) to forward scatter, this version of the FORTRAN program generates output at both pin faces, i.e., the bottom and top pin face. Rays gathered at the bottom of the pin cannot indicate whether they reflected from the slot or from the pin side wall, they merely indicate that reflections occurred in mid travel. Rays gathered at the top of the pin face, however, do indicate reflections from the slot, because they back scatter from the top plane of the slot, indicated by their short total length of travel.

5.d FORTRAN program Results

5.d.1 Computational requirements for visualization of results

Once the data is post processed with a particular receiver and density grid pattern, it must be output for plotting on screen using PV-WAVE data visualization software.

The computational requirements are not as processor intensive as the main process, but do require graphics capable computers to run PV-WAVE plotting software. Computers with at least 24 Megs of memory and at least 2 megs of video ram is a base requirement, much more is required for 3-D visualization.

5.d.2 Data processing for results to be visualized

The post-processing algorithm discretizes the large number of rays picked up at a particular depth section into values at discrete probe nodes on the receiving grid. The thickness of the depth section is entered into the program through the input file called "postin.dat". More then one depth section can also be chosen to be plotted by entering the pin length discretization number, which breaks the pin up into that number of equal thickness sections. Resulting data from the post-processing FORTRAN program "post3.for" is output to "postout.dat" in a single column. For example, if the C-scan is 10 by 10 in resolution (10 pixels horizontal by 10 pixels

vertical), then the "postout.dat" file would contain 100 data entries, each ranging in values of zero or larger. For more scans resulting in more than one depth slice, the number of rows written are the nodes in a single slice by the number of total slices generated. A PV-WAVE procedure file "post3.pro" reads in the "postout.dat" file and plots it as a grayscale image slice composed of pixels (single color point on the screen) ranging in-between the minimum and maximum values for each slice.

Chapter 6 Results and discussion

6.a A-scan (model vs. Calibration pin)

6.a.1 Differences between the calibration pin and model A-scans

Figure 22 shows the A-scan resulting from the model compared to the A-scan of the calibration pin shown in figure 23. The three major peaks correspond to the three depths from which large amounts of rays reflected. The number of rays that returned to the probe from a particular depth represents the amplitude of the signal at that depth. Since the model's basis is that a beam is composed of a large number of rays, the number of rays reflecting from a particular depth correlate to the amount of energy of a beam that reflects at that depth.

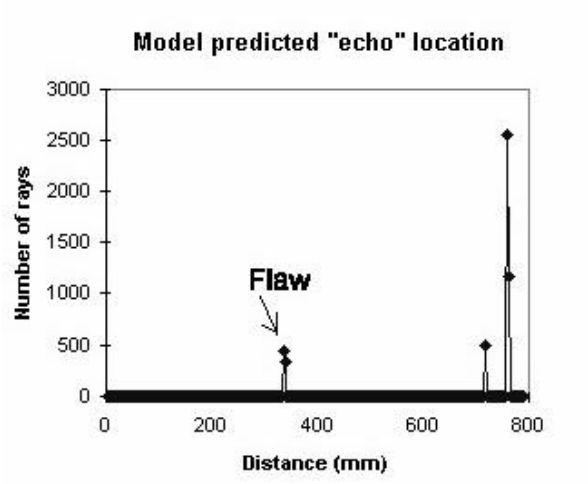

Figure 22 shows a model A-scan of the slag inclusion flaw

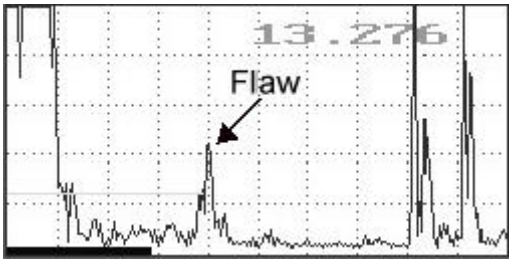

Figure 23 is an A-scan obtained from the calibration pin when the transducer is positioned to detect a reflection from the slag inclusion.

6.b C-Scans (model vs. calibration pin)

Figure 24a shows the C-scan results of the model for a low-resolution grid case of the slag inclusion. The gray scale represents the number of reflections that arrived at the scanning surface within the time gate, the larger the number of arrivals, the darker the shade. The results indicate the general location of the flaw in a cross-section perpendicular to the axis of the pin. Figure 25 is the corresponding C-scan of the calibration pin using a gate located about the echo from the slag inclusion. The differences in the images can be attributed to the multi-planar nature of the flaw in the calibration pin. In reality the flaws are not flat as represented by the model. Rather the flaw has a faceted surface, which scatters parallel rays in very different directions.

Another difference is that the simulated C-scan results from a much coarser grid of data points than the C-scan of the calibration pin. An effort has been made to use a "simulated" time gate that corresponded to that used in the calibration pin scan. As shown in figure 24b, the results of the same C-scan using a medium-resolution grid for a shorter time gate, which corresponds to that of the calibration pin C-scan shown in figure 25. Figure 24b is a top-down view of the pin, with the dark area at the very top representing the crack modeled, the white inner area representing the scanning surface (six inches (15.24cm) in diameter), and the gray outer area representing the main pin (nine inches (22.86cm) in diameter).

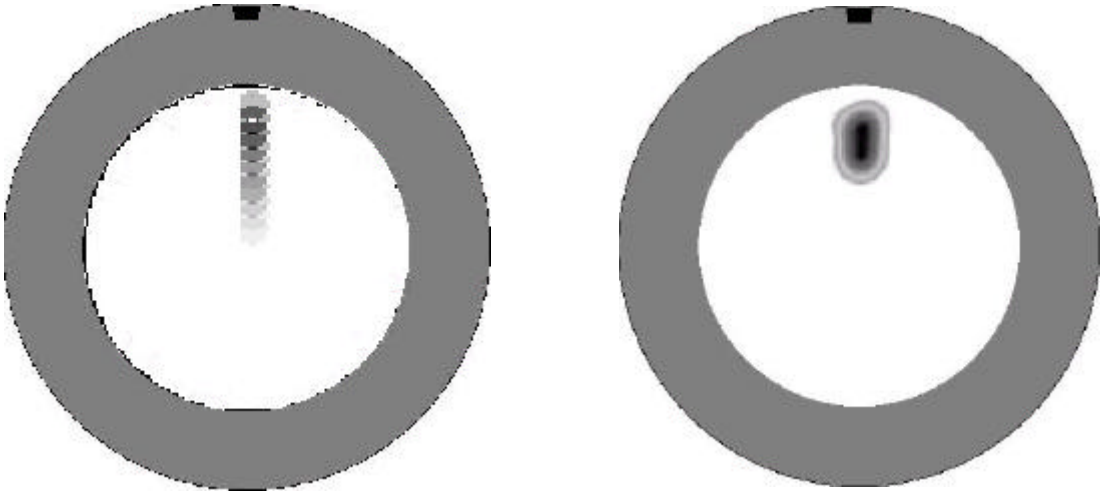

Figure24 a) shows the low-resolution C-scan of the slag inclusion flaw predicted by the model, b) shows the same predicted C-scan at a medium resolution and corresponding calibration pin time gate. Images drawn with PV-WAVE

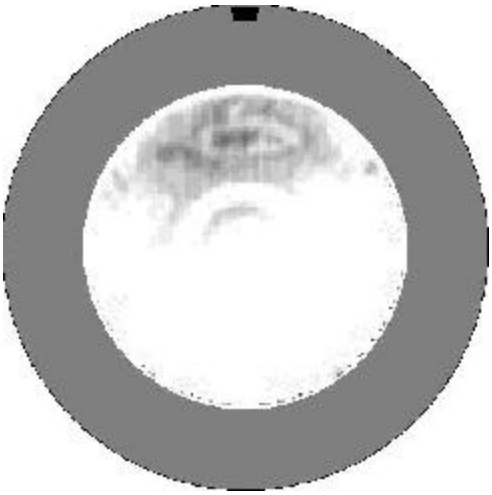

Figure 25 shows the C-scan of the same slag inclusion performed on the calibration pin using field C-scanning robotic system.

6.c Case trials for the model for wear groove

The results at this stage for the forward scatter indicated that the difference between crack and groove could be seen in the detected rays at the bottom face of the pin. However, the groove must be symmetrical around the pin, a groove on one half of the pin would not be differentiable from a crack that long. Figure 26a shows that the virtual point probe generating the rays is located at the center of the top pin face. Figure 26b shows the image resulting from forward scattering at 72.5 degree down angle with the groove at 13.3 to 13.8 inches (33.78 to 35.05cm), and a .5 inch (1.27cm) deep slot cut out. Figure 26c shows the corresponding small crack (same dimension as crack used above for C-scans) at 13.3 inches (33.78cm) from top of pin. The difference between the two images is observed because the rays that have not been blocked by the crack hit the pin bottom to form a semi-circle, but those same rays were all blocked by the groove. This is the why the smaller circles in figure 26 a and figure 26 b are of different radii. The circle observed in figure 26 b is formed by the rays symmetrically hitting the groove's cylindrical wall.

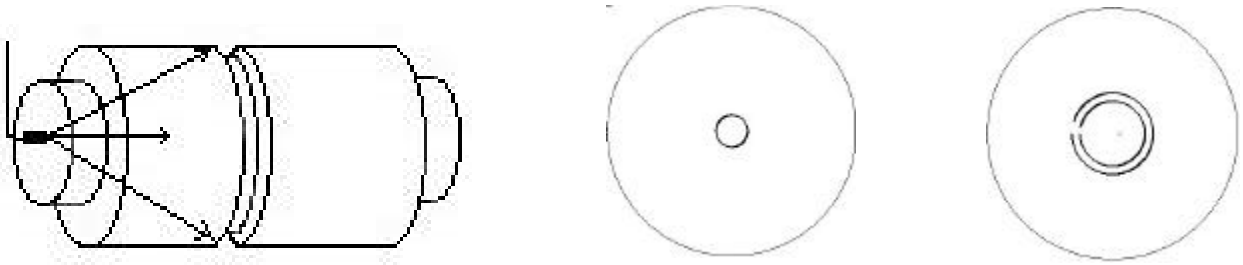

Figure 26 a) shows the probe location, b) the resulting forward scatter image for the groove, and c) the forward scatter image for the crack

Chapter 7 Conclusions

7.a Summary

In an attempt to improve the ultrasonic inspection of steel bridge pins, an approach for in-situ ultrasonic C-scanning of the pin has been developed by the Virginia Transportation Research Council. The C-scan images obtained using a contact longitudinal transducer are difficult to interpret. The transducer generates a beam, which experience considerable beam spread within the pin causing complex reflection patterns. A computer model has been developed to simulate ultrasonic wave propagation and determine data detection patterns to better describe flaws in these fracture critical members.

The raytrace model that has been developed in this study uses a kernel to generate and reflect rays inside of a geometrical model of a steel pin. Three interface algorithms were overlaid on top of the kernel to generate specific type of output corresponding to an A-scan, C-scan, and forward scattering detection of flaws. The A-scan algorithm generates a plot of amplitude versus length for a particular source point. The C-scan algorithm generates an image of the reflections detected along a cross-section perpendicular to pin axis at a particular depth. The forward scattering algorithm shows reflections from groove and cylinder sidewalls detected at the bottom pin face.

There are two types of flaws modeled within this study. One, a Z-plane arc shaped pie wedge flaw (crack), which simulated a shear crack (surface and sub-surface slag inclusion.) This situation model seemed to confirm the model A-scan and C-scan results matching to A-scan and C-scan tests of the calibration pin. Second, a groove/slot keyed around the main cylinder of the pin. The simulated groove showed to have different reflection characteristics then the crack when used within the forward scatter imaging. A symmetric groove resulted in a symmetric circle of rays detected at the bottom pin face, while the crack resulted in a broken circle of rays detected at the bottom face because some rays were being blocked by the crack.

7.b Conclusions: Improved ultrasonic inspection of steel bridge pins

The present procedure for ultrasonic inspection of a bridge pin relies on using just the A-scan data. Since it is often difficult from A-scan data alone to assess the size of a flaw, additional data

were obtained using an ultrasonic C-scan procedure developed by VTRC. However, for both the A-scan and C-scan based inspection, it is difficult to properly interpret the data result from scattering of a diverging ultrasonic beam. The model developed here will allow the inspector to simulate the A- or C-scan results that would be obtained for suspected flaws. By comparison of the actual A- or C-scan results with those simulated, as shown in figure 27, a better interpretation of the condition of the pin is possible.

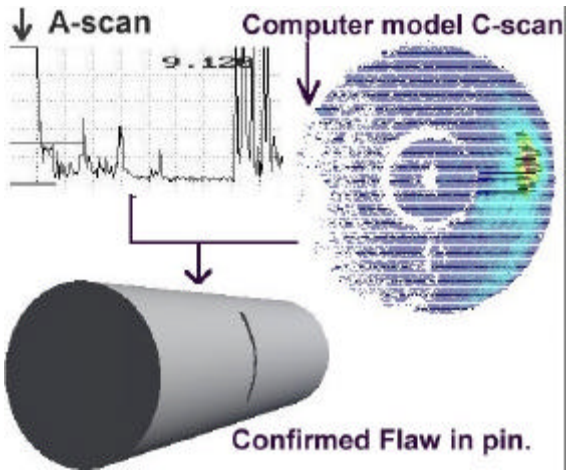

Figure 27 Confirming and detailing flaw condition using field scanning and modeling results

7.c Recommendations and future work

7.c.1 Phase interactions

Phase interactions could be incorporated into the main kernel, which could constructively/destructively interfere with other rays that are arriving next to the detected ray keeping track of time-of-flight and attenuation. This would result in a better representation of ultrasonic wave propagation in steel pins for the raytracing model.

7.c.2 EMAT incorporation

One might also research the use of EMATs (Electro-Magnetic Acoustic Transducers) which excite radially polarized horizontal shear (SHl) waves below the pin face. One could model EMAT raytracing more accurately with this kernel because no mode conversion occurs during radially polarized SH waves propagating in the pin.

7.c.3 Denser forward scatter

For the forward scatter algorithm, one could use more then a single down angle for the emanating cones of rays. With more angles, greater ray density of non parallel rays can be achieved, allowing more rays to be detected at the bottom, giving a higher resolution forward scatter images.

7.c.4 Language barrier

With modifications to the kernel code, it would be possible to locate flaws from C-scans for other geometric forms with a strong degree of confidence. It is advised that the next version of the models be implemented using another language that performs better file and resource handling.

7.c.5 Improved smaller field C-scanning system.

As the results of this project are being discussed, new and smaller integrated C-scanning systems are being developed. A system specifically designed for inspecting bridge pins has been proposed, shown in figure 28. Unlike the field C-scanning system used for this project, this proposed system is a micro drive system, which mounts directly onto the threaded end of the pin. The transducer used with this system will be a radially and horizontally polarized electromagnetic acoustic transducer. The EMAT will "attach" to the pin because of the magnets used for exciting the ultrasonic wave and be manipulated over the end of the pin surface using motor for indexing circularly and a second motor for translating radially to accomplish the C-scan.

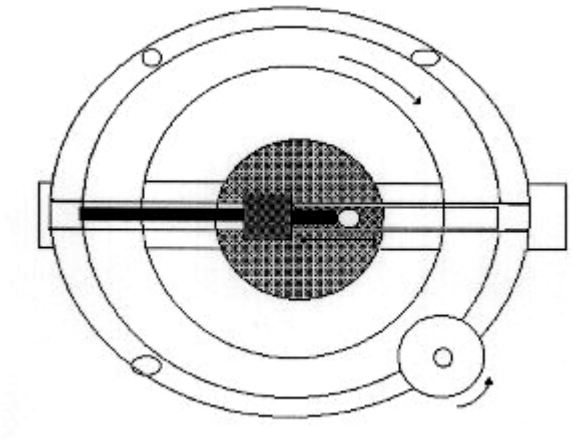

Figure 28 Proposed radial scanning C-scanning system.

References

Lozev, M.G., Clemena, G.G., Duke, J.C., Sison, M.F., and Horne, M.R., "Acoustic Emission Monitoring of Steel Bridge Members", Final Report, Virginia Transportation Research Council, Charlottesville, Virginia, April 1997

McCurdy, M., "Ultrasonic Inspection of Pin Assemblies in Bridges"
Materials Evaluation, American Societies for Nondestructive Testing, Inc., December 1989

Harland, J.W., Purvis, R.L., Graber, D.R., Albrecht, p., and Flournoy, T.S., "Inspection of Fracture Critical Bridge Members", Federal Highway Administration, McLean, Virginia, September 1986

Harm, E.E., and Washer, G., "Improving the Correlation of Ultrasonic Testing Results to the In place Condition of Bridge Suspension Pins", Problem Statement 95-D-33, Illinois DOT, Springfield, Illinois, October 1993

Finch, K.J., Freeman, M.P., and Snyder, S., "NDT(UT) Inspection and Data Management for Bridge Pins and Trunnions", Structural Materials Technology An NDT Conference, New Jersey DOT, Atlantic City, New Jersey, February 1994

komsky, I.N., and Achenbach, J.D, "A Computerized Imaging System for Ultrasonic Inspection of Steel Bridge Structures", Structural Materials Technology An NDT Conference, California DOT, San Diego, California, February 1996

Achenbach, J.D., Komsky, I.N., and Stolarski, P.J., "A Self-Compensating Ultrasonic System for Flaw Characterization in Steel Bridge Structures", Structural Materials Technology An NDT Conference, New Jersey DOT, Atlantic City, New Jersey, February 1994

Miller, W.J., and Chaney, M.K., "NDT of Bridge Pins on PennDOT Structures"
Structural Materials Technology An NDT Conference, New Jersey DOT, Atlantic City, New Jersey, February 1994

Gessel, R.D., and Walther, R.A., "Ultrasonic Inspection of Bridge Pin and Hanger Assemblies"
Structural Materials Technology An NDT Conference, California DOT, San Diego, California, February 1996

Thomas, G., Benson S., Durbin, P., and Del-Grande, N. "Nondestructive Evaluation Techniques for Enhanced Bridge Inspection", Quantitative Nondestructive Evaluation 93 Conference, Brunswick, Maine, August 1993

Electric Power Research Institute, "Raytrace", http://www.karta.com, 1998

Kolsky, H., Stress Waves in Solids", Dover Publications, Inc., New York, N. Y., 1963

ASM Handbook, Volume 17. "Nondestructive Evaluation and Quality Control", ASM International, Fourth printing, January 1996

Appendix A

Definition of an A-scan

Ultrasonic A-scan examinations generate quick results. An A-scan plots signal amplitude against time. Figure 29 shows a sample A-scan of the bridge pin. The initial peak represents the signal reflected from the pin face and top shoulder. The second peak, the flaw reflections, are in-between the top shoulder reflection and the bottom shoulder reflection. Once past the plate it propagates through the steel pin, reflecting from any geometric boundary or any material discontinuity.

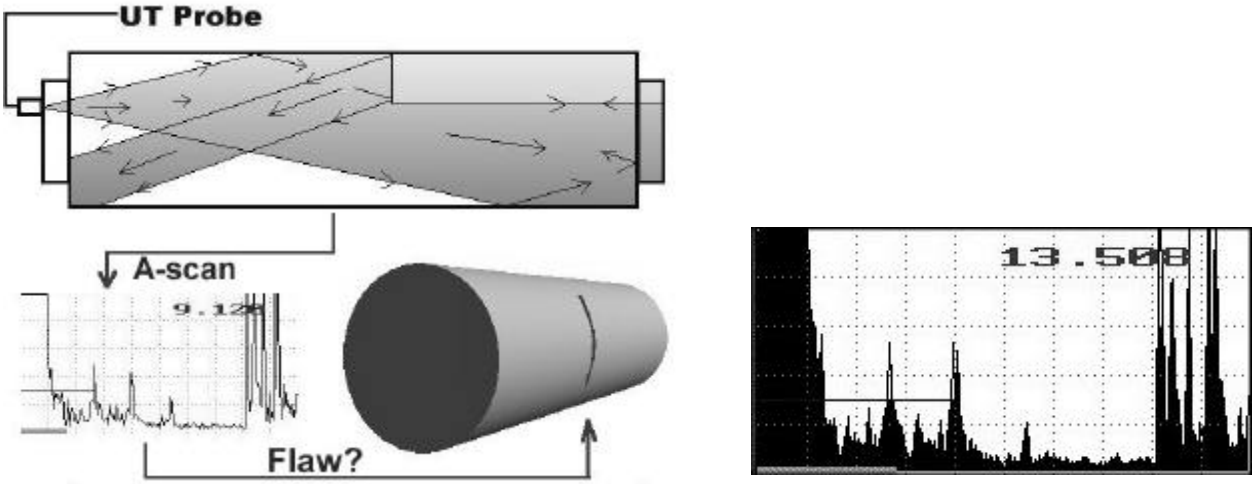

Figure 29 a), b) shows the results of A-scan testing performed on the bridge pin #12

The distance to flaw is the total distance traveled divided by two. This is because the signal must travel a certain distance out then reflect and travel back some distance, therefore averaging by 2 gives an approximate distance to flaw. At times the distance to the flaw may not be the distance from probe point on pin face to flaw. Reflections being angled, total distance traveled divided by 2 is larger then distance directly from probe to flaw. Accurate measurements can only be obtained when flaws are directly beneath the probe and return signals normal to the surfaces.

The larger the flaw, the larger the area available for reflection to occur, causing a greater part of the intercepted beam to be reflected. Total reflection of a beam/signal indicates that the flaw has a cross-sectional area equal to or larger than the cross-sectional area of the beam. A total reflection also indicates that the flaw is composed of an empty (air) cavity in the continuous

material, which is why no signal is transmitted through, but is totally reflected. For this reason, the correct transducers must be used in the ultrasonic A-scan examinations. A flaw near the lateral surface of the pin will require the use of wide-angle beam probes, while a focused beam probe can easily detect a flaw closer to the center of the pin diameter. The beam spread of a focused beam probe is small thus alleviating other boundary reflections such as threads, wear grooves, reflectors near the outer diameter of the pin from being detected in the A-scan.

Appendix B

Definition of C-Scan

C-scans are one of the most time consuming of all the NDE methods. Once scanning equipment is setup, it can take over an hour to scan an area of 6 inches (15.24cm)by 6 inches (15.24cm), to obtain high definition images of flaw reflections. A C-Scan is a planar view of flaw reflections at a particular depth. C-scan images look much like a top-down cross-sectional view of the pin at flaw depth. A C-scan is constructed by gating an A-scan signal, then scanning the transducer across the pin face, and plotting that gated signal as a colored pixel in its corresponding position on the image. The amplitude of the peak signal is discretized and assigned a color bar, where 0% amplitude would be a blue colored pixel, while 100% amplitude would be a red colored pixel. Figure 30 illustrates a sample C-scan.

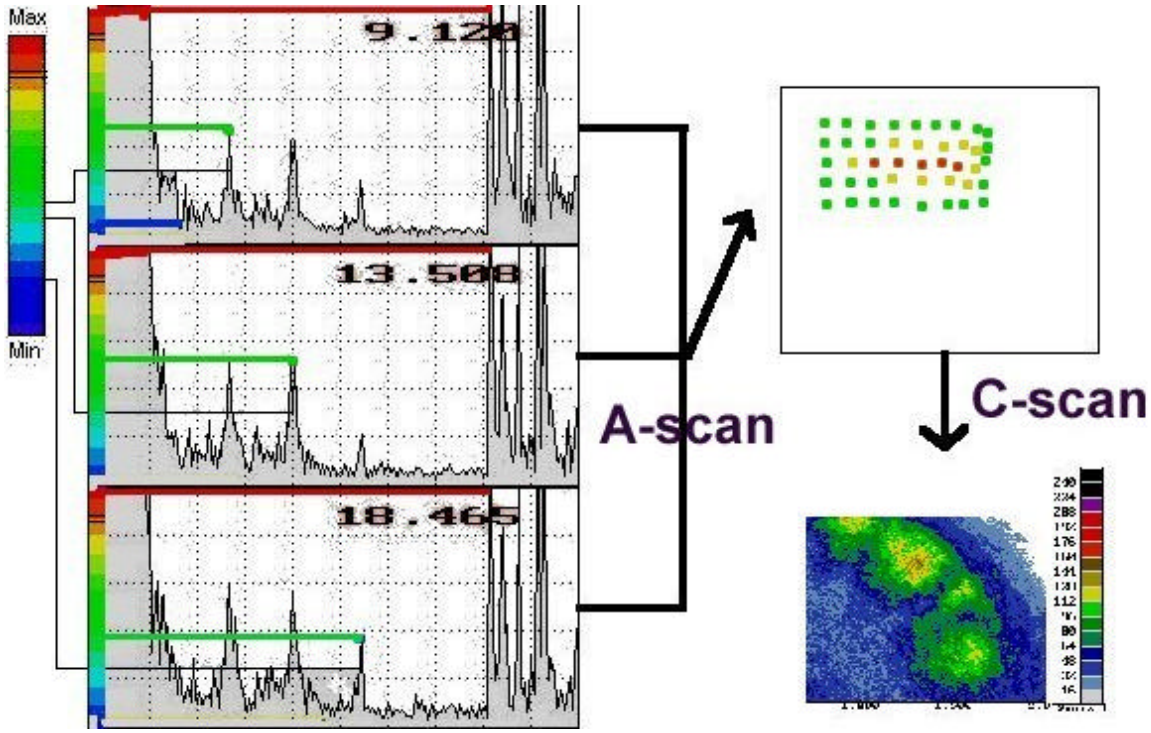

Figure 30 Illustration of the formation of a C-scan from A-scans taken at a particular depth

Appendix C

Beam Spread Equation

To calculate the required range of angles of beam spread for the model, the inspector must use equation 6 [ASM Handbook 1996] shown, with known probe parameters. To satisfy this equation the following list of parameters must be input: probe frequency, and probe diameter.

Where the wave speed is entered in meters per seconds (5900m/s for longitudinal waves in steel), frequency in megahertz (5 MHz), and the diameter in millimeters (13mm). For example, the sample values given result in a beam spread angle of 12.5 degrees from the vertical

$$\Phi = 2\,Sin^{-1}\left[\frac{1.2\,x10^{-3}\,(Wavespeed\quad)}{(\ freq\ )(\ diameter\quad)}\right]$$

Equation 6 Beam spread equation

Appendix D Algorithm Flow-Charts.

A-scan [Ascan.cht]

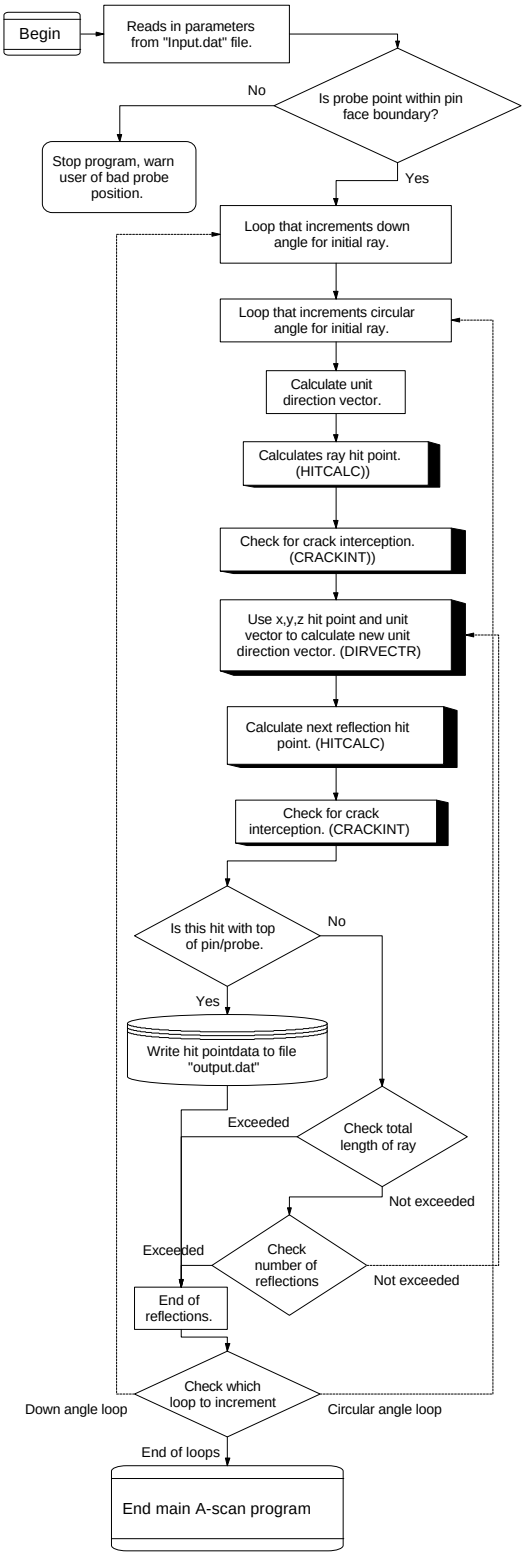

C-scan [Cscan.cht]

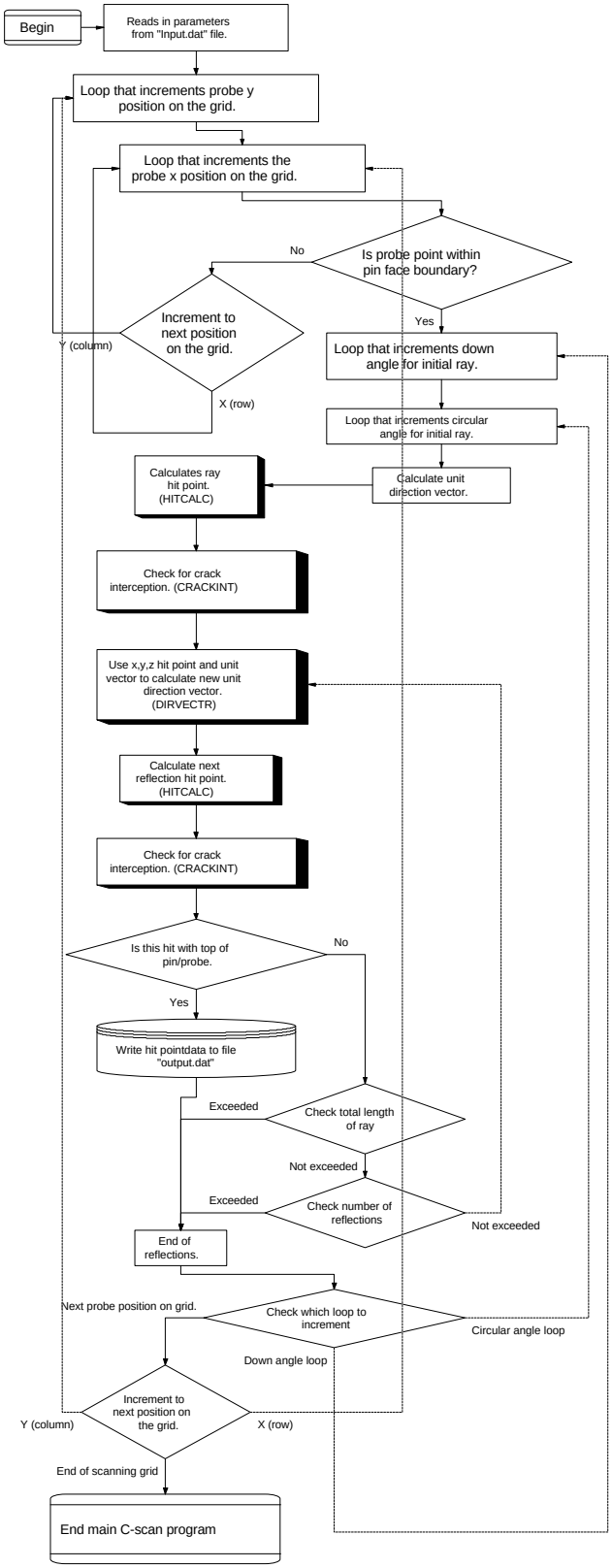

Forward scatter [Fwdscatr.cht]

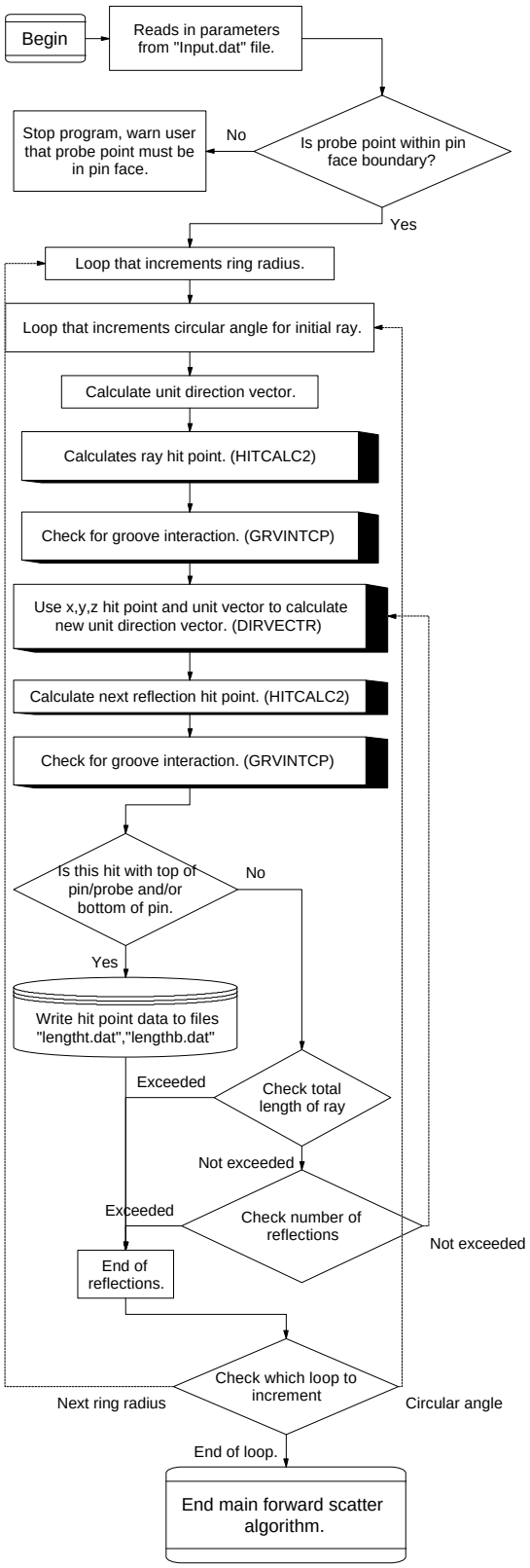

Direction vector calculation [Dirvectr.cht]

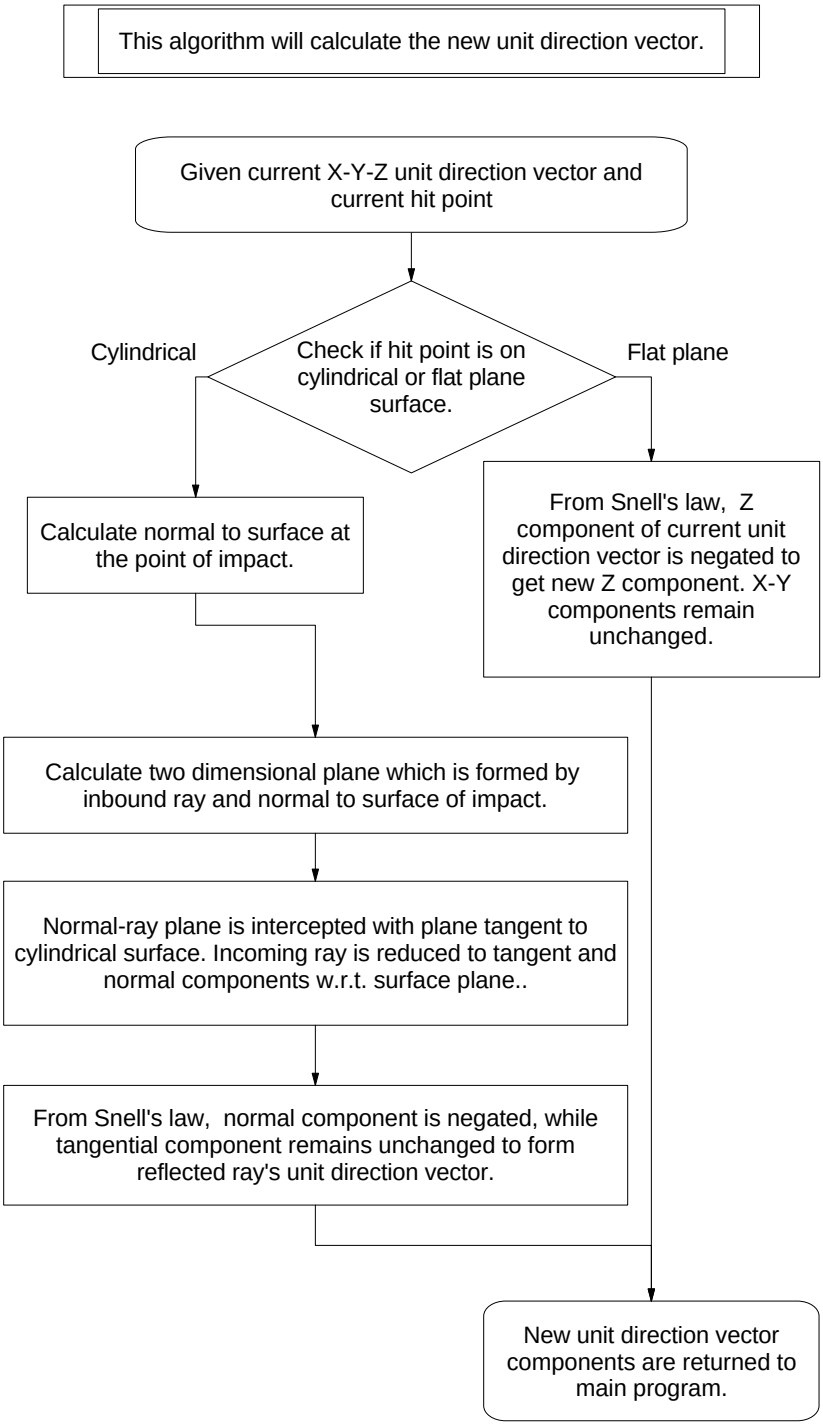

Hit point calculation [Hitcalc.cht, Hitcacl2.cht]

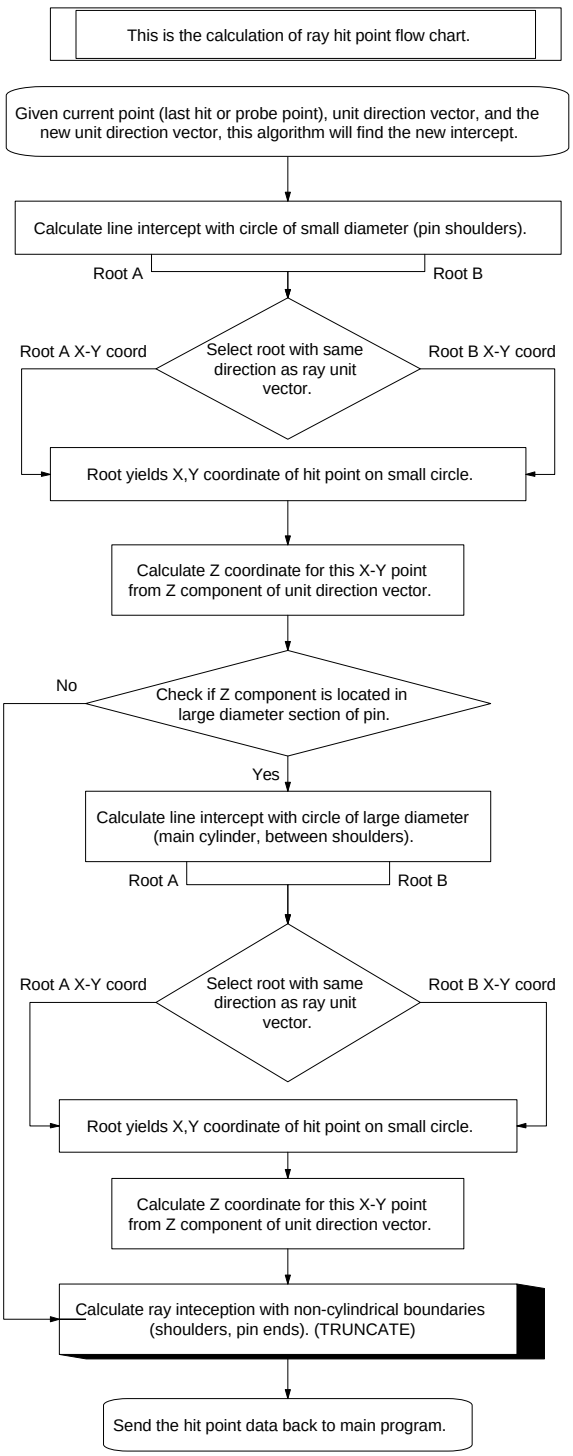

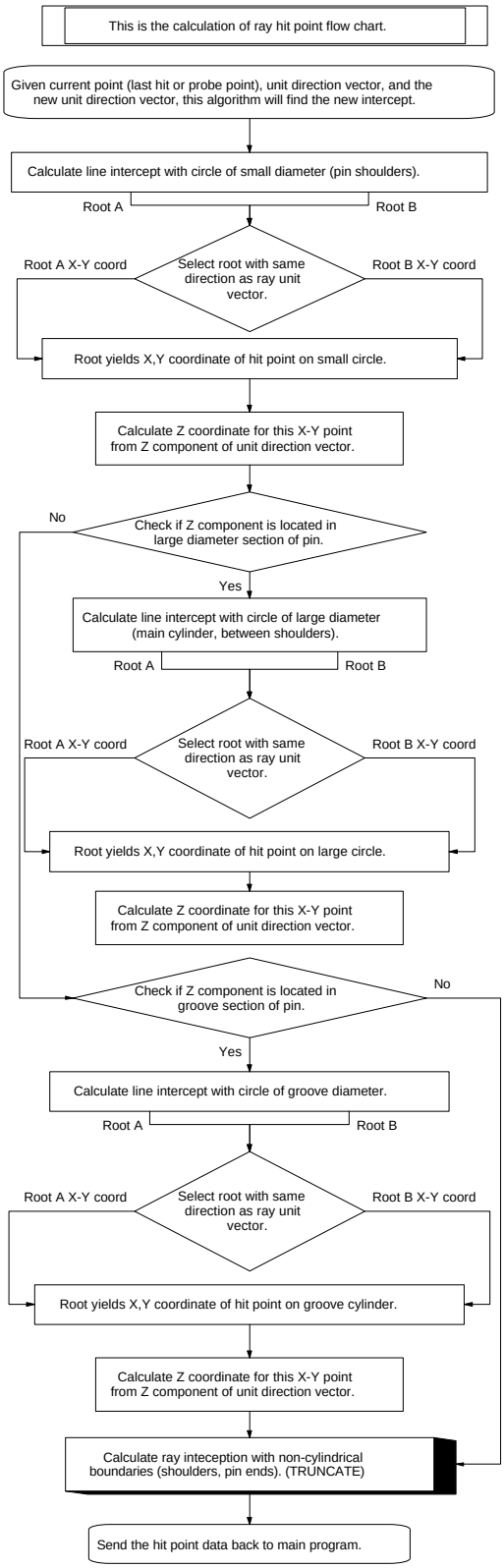

Truncation [Truncate.cht]

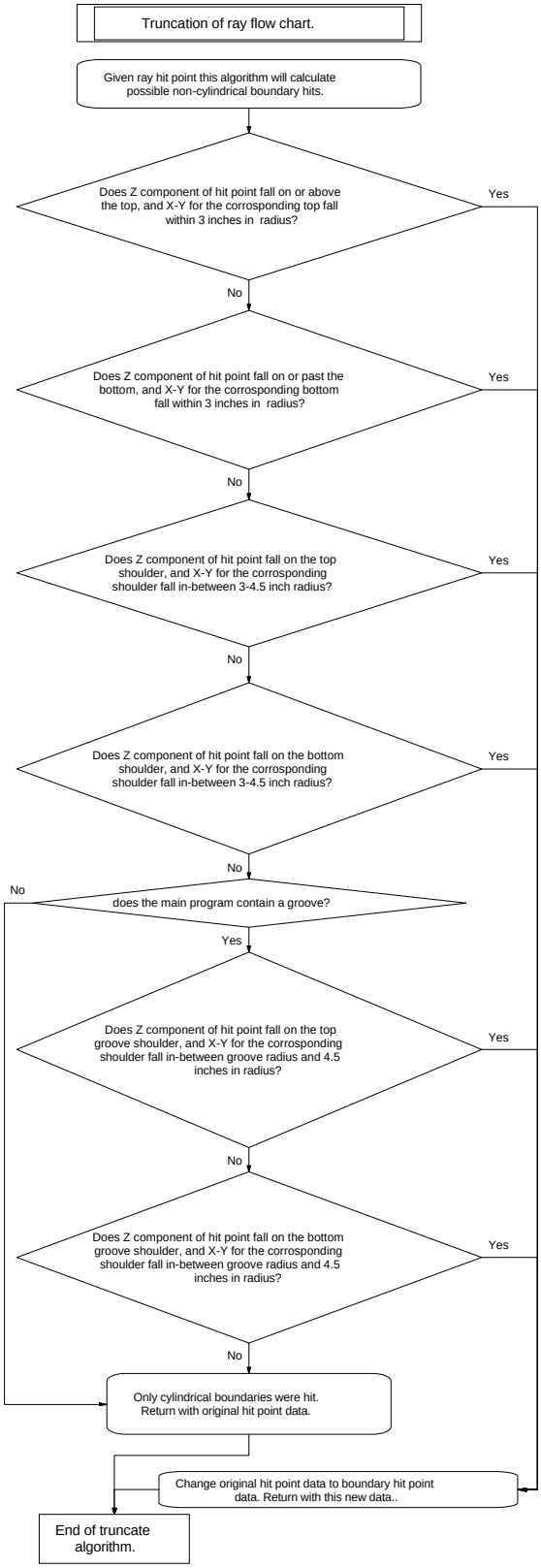

Flaw interception [Crackint.cht, Grvintcp.cht]

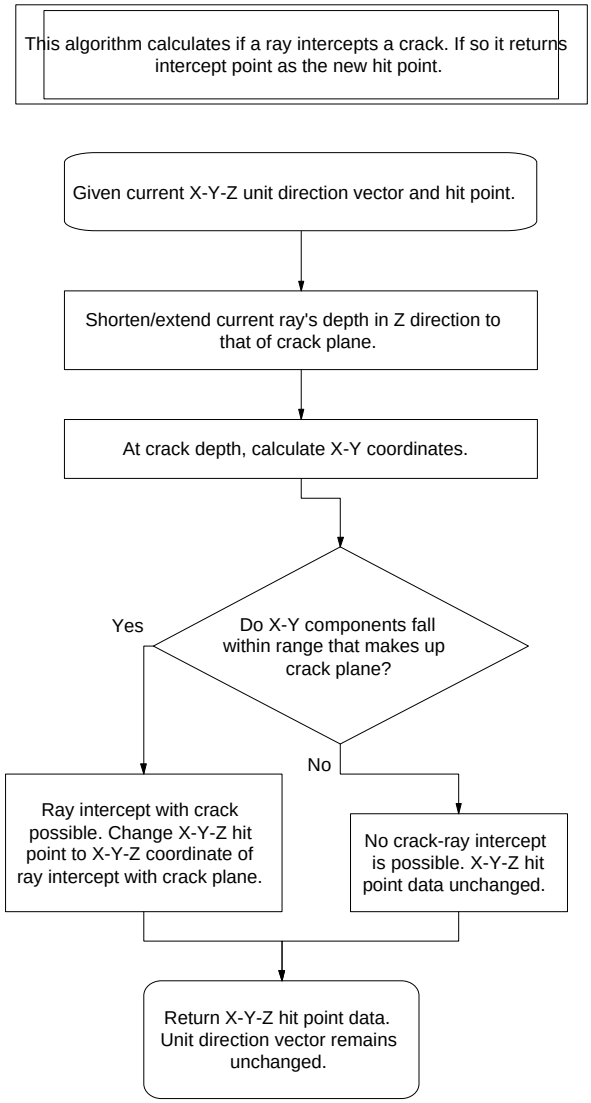

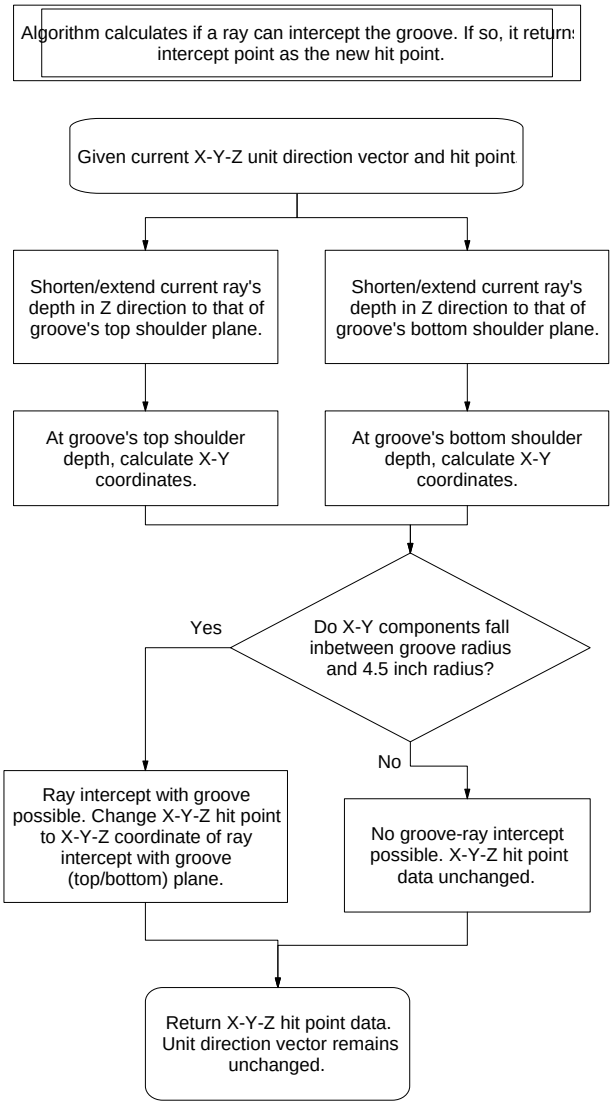

Appendix E

Working FORTRAN program codes

To acquire these files please contact Dr. John C. Duke, Jr.

FORTRAN code for the A-scan algorithm. [Ascan.for]

FORTRAN code for the C-scan algorithm. [Cscan.for]

FORTRAN code for the post-processing C-scan code's data output. [Post3.for]

PV-WAVE Procedure file for plotting the post-processed output data. [Post3.pro]

FORTRAN code for the forward scatter algorithm. [Groove.for]

Java code for viewing Groove.for's output data file. [Sam.java, requires MainCanvas.java to run]

Appendix F

Input1.dat file for the A-scan FORTRAN program.

BOTTOM: bottom of pin(31 inches (78.74cm))

LENDS: length of pin ends(3.5 inches (8.89cm))

RADSML: radius of small cylinder (3 inches (7.6cm))

RADLAR: radius of large cylinder (4.5 inches (11.43cm))

MAXREF: maximum reflection number (10)

LENMAX: maximum length to begin cutoff (32 inches (81.28))

PROBX: probe x coordinate location

PROBY: probe y coordinate location

PROBZ: probe z coordinate location [always zero]

SPRBEG: downward ray begin angle (68 degrees)

SPREND: downward ray end angle (89.9 degrees)

DWNINC: downward ray increment angle (.5 degrees)

PHIBEG: circular ray begin angle (0.0 degrees)

PHIEND: circular ray end angle (359.99 degrees)

CIRINC: circular ray increment angle (.2 degrees)

CRANGS: crack begin angle (-3.2 degrees for subsurface flaw)

CRANGL: crack end angle (3.2 degrees)

CRRADS: crack small radius (4.19 inches (10.64cm))

CRRADL: crack large radius (4.44 inches (11.28cm))

CRHIGH: crack length in z plane (13 inches (33.02cm))

PDIAM: probe diameter for A-scan (.545 inches (1.384cm))

Appendix G

Input2.dat file for the C-scan FORTRAN program.

BOTTOM: bottom of pin

LENDS: length of pin ends

RADSML: radius of small cylinder

RADLAR: radius of large cylinder

MAXREF: maximum reflection number

LENMAX: maximum length to begin cutoff

SPRBEG: downward ray begin angle

SPREND: downward ray end angle

DWNINC: downward ray increment angle

PHIBEG: circular ray begin angle

PHIEND: circular ray end angle

CIRINC: circular ray increment angle

CRANGS: crack begin angle

CRANGL: crack end angle

CRRADS: crack small radius

CRRADL: crack large radius

CRHIGH: crack length in z plane

N: x row incrementation number [x-grid value]

P: y column incrementation number [y-grid value]

PDIAM: probe diameter for C-scan

XSTART: x incrementation start #

YSTART: y incrementation start #

Appendix H

Input3.dat file for the forward scattering FORTRAN program.

BOTTOM: bottom of pin

LENDS: length of pin ends

RADSML: radius of small cylinder

RADLAR: radius of large cylinder

MAXREF: maximum reflection number

LENMAX: maximum length to begin cutoff

PROBX: probe x coordinate location

PROBY: probe y coordinate location

PHIBEG: circular ray begin angle

PHIEND: circular ray end angle

CIRINC: circular ray increment angle

CRANGS: crack begin angle

CRANGL: crack end angle

CRRADS: crack small radius

CRRADL: crack large radius

CRHIGH: crack length in z plane

PDIAM: probe diameter for C-scan (.545 inches (1.384cm))

GRVTOP: the z position of top of groove (13 inches (33.02cm))

GRVBOT: the z position of bottom of groove (13.5 inches (34.29cm))

GRVDPT: the radial depth of the groove (.5 inches (1.27cm))

THETA: the central down angle for the probe (75 degrees)

RINGOT: the number of rings per transducer (15 rings)

Appendix I

Results of the Radford Memorial Bridge pin situation.

While this model was in mid development, the chief bridge engineers thought it best to reinforce the suspect pins just incase our (complex) suspected flaws grew.

Vita

Sanjiv D. Parikh was born on the 1st of September, 1972, in Baroda, India. He moved with his family to Lynchburg, Virginia, USA in 1982. From E. C. Glass, he received his High School Diploma in 1989. He earned his Associates in Science in Electrical and Computer Engineering from Northern Virginia Community College (NOVA) in summer of 1993. He graduated from Virginia Polytechnic Institute and State University, Blacksburg, with a Bachelor's in Engineering Science and Mechanics with a concentration in Biomedical Engineering, in fall of 1995.

He is a member of Dean McPherson's Graduate Committee on Research in the College of Engineering at Virginia Tech. He is a member of the Virginia Tech CAVE SLUGs. He considers research and learning a great part of his life and strives towards his goal of contributing to the future of technology. He enrolled in the Ph.D. program at Virginia Tech in fall 1998 to pursue his dreams of prototyping new biofeedback devices. He has developed a deep interest in computing resources. He is mechanically inclined and tries to apply his engineering knowledge to every day problems.

He wishes to enjoy academics as well as the outdoors. He has enjoyed bicycling since 1987. He has recently become a fan of tubing and river recreation. Since he has none, he enjoys and appreciates the musical talents of others. He believes that life should be enjoyed to the fullest at every chance one gets.